Monitoring food structure in plant protein gels during digestion: Rheometry and Small Angle Neutron Scattering studies

Maja Napieraj, Annie Brûlet, Evelyne Lutton, Urielle Randrianarisoa, Adeline Boire, François Boué

Monitoring food structure in plant protein gels during digestion: rheometry and Small Angle Neutron Scattering studies

Maja Napieraj[a], Annie Brûlet[a], Evelyne Lutton[b], Urielle Randrianarisoa[a], Adeline Boire[c], François Boué[a]

[a]. *Laboratoire Léon Brillouin, UMR12 CEA-CNRS, Université Paris- Saclay, CEA-Saclay, F-91191, Gif-sur-Yvette, France*

[b]. *INRAE, Université Paris-Saclay, UMR518, Institut des systèmes complexes, ISC-PIF, 75013 Paris France.*

[c]. *Unité Biopolymères, Interactions et Assemblages, UR1268 INRAE, F-44316, Nantes, France.*

Abstract

We studied rheology and nanostructures (by small angle neutron scattering) of heat-set canola seed protein gels, containing cruciferin and napin, prepared at pH 8 and pH 11. We focused on gastric and intestinal digestion of ten mm pieces, mimicking human gastro-intestinal tract. Stronger gels, prepared at pH 11 (above the IEP, isoelectric points, of both proteins), retained local folded and compact conformations, close to native. Preparation at pH 8 (below napin IEP but above cruciferin one), could destabilize conformations due to charge differences of the proteins. For preparation pH 8, proteins were almost unfolded, and the gel softer. In gastric digestion, modulus decreased for pH 8 gels, but surprisingly, increased for pH 11. We propose a competition between unfolding, increasing local interactions (hence the modulus), and enzymatic scission. Scission could be less efficient for pH 11, with less unfolded proteins and higher crosslink density, hindering enzymatic diffusion. Additional interactions could result from crossing one or two IEPs, towards gastric pH 2. For intestinal digestion, the two gels behave similar (proteins re-compaction and modulus decrease). Beyond loss of submicronic connectivity, external erosion of the gel for largest times is observed, but less on SANS, which involves the centre of the piece.

1. Introduction

Proteins are crucial macronutrients in human diet, providing essential amino acids to meet functional and structural needs of the human body[1,2]. Moreover, they also take part in the structure of food, whether they are ingested in majority, or not. This capacity is, in particular, due to their ability to form structures at multiple spatial scales, e.g. gels – solid-like materials holding the properties of both a solid and a liquid[3].

There is a great potential in obtaining a variety of protein gels with different structures, dependently not only on the nature of the proteins itself, but also on the way their network is formed. The gel formation requires a driving force, sufficient to initiate at least partial unfolding of native protein structures, enabling crosslinking between different molecules and their following aggregation, finalized by generation of a three-dimensional network spanning the entire volume of the sample[3]. Many gel-forming food proteins such as ovalbumin, whey or plant proteins are globular proteins, holding rather compact and well-defined tertiary structures, and their aggregation-gelation process is often induced by a heat-treatment[4]. Such a physical gelation of globular proteins and a stabilization of the formed gel involve hydrogen-bonding, hydrophobic interactions and covalent cross-links[3]. The protein network structures, obtained only on the way of the temperature gelation, can own vastly different morphologies and physical properties, depending on the protein source and the processing conditions during gelation; the pH, temperature, and protein or salt concentration influence the strength of the short- and long-range attractive interactions in the formed system[5,6]. For example, a decreased repulsion, caused by salt addition or by approaching the pH of protein isoelectric point (IEP), can promote more disordered gel networks[7]. Offering a strong case of how different types of food processing can alter its microstructure, proteins can be also good examples of how structure influences food digestion. On the one hand, the processing can facilitate the intestinal digestibility of some of the plant-based foods, by, e.g., reducing the effect of anti-nutritional factors such as protease inhibitors, tannins or phenolic compounds, as shown in many studies[8,9,10,11]. On the other hand, it may slow down the protein hydrolysis, by e.g. hindering an enzyme's penetration through more densely aggregated structures present in the food matrices. It is known that, in general, solid-like foods, such as protein gels, undergo more complex and longer processes of digestion, compared to liquid foods, since they require disintegration to much smaller particles[12]. The structure of protein food constitutes hence as an important factor in its nutritional quality, with an impact on the protein digestibility, the

kinetics of proteolysis and the resulting amino-acids bioavailability, having therefore potential metabolic consequences[1,13,14,15].

The food structure's impact on the protein digestion was presented in an *in vivo* study on mini pigs, where different rates of their leucine plasma content, indicating different protein digestion rates, were recorded upon digestion of differently-structured milk products[16.] Several *in vitro* studies, involving animal-sourced protein gels (from whey and egg white), associated their densely cross-linked gel structures with slower rates of the protein hydrolysis and a nutrients release during simulated gastric digestion[17,18,19]. Such microstructures can hinder the gastric digestion by not only slowing down the proteolysis through limited enzyme's diffusion, but also by influencing the enzyme kinetics[20]. Some additional studies on soy and pea protein gels showed that the protein source, by altering the gel structure, can also greatly influence the gastric protein digestibility[21]. On the protein structure level, the specific secondary and tertiary structures of the molecules can constitute as inherent structural hindrances, limiting the accessibility of the digestive enzymes to peptide bonds, e.g. due to large number of disulfide bonds, stabilising compact globular structures.

The gastric mixture of pepsin and hydrochloric acid creates a first step of the protein chemical hydrolysis. The activity of pepsin is highly dependent on the pH conditions, with a maximum value between pH 1.5 and 2.5[22,23,24]. The acid uptake into the food particle, specific for the type of food[25], is therefore important for lowering its initial pH (usually much higher than in the stomach) and optimizing the pepsin's activity[26]. Additionally, the strongly acidic environment favours protein denaturation, which may facilitate their digestion by increasing the access to substrates for the enzyme. Pepsin has a broad amino-acid specificity, with a preference for hydrophobic residues[27]; it breaks down ingested peptide bonds, resulting in the formation of a mixture of polypeptides, oligopeptides, and amino acids[25,28]. Subsequently, the gastric chyme is transported to the small intestine, where the protein digestion is continued by the action of pancreatic proteases (trypsin, chymotrypsin, elastase and carboxypeptidases) in the optimal pH around 7, at which pepsin is inactivated[24]. The pancreatic proteases display a wide specificity and further degrade remaining polypeptides into free amino acids or di- and tripeptides, being small enough to be released into the blood[25].

Both the pH environment of each digestive step and the pH of the protein gel itself affect the digestion process. Dependently on the protein charge/how the internal pH differs from the isoelectric point, the protein gel will experience swelling or shrinking/deswelling. The lowest swelling potential occurs when close to the IEP of a given protein[29], and when crossing this

zero-charge point, even contraction can take place[25]. It can be thus expected that swelling will facilitate digestion by allowing a convective influx of the acid and the enzymes into the gel, and opposite behavior in the case of shrinking.

Due to the increased interest in incorporating plant protein sources, such as seeds, legumes or cereals, in human nutrition, there is a need for a better understanding of processes involved in the digestion of structured foods made from such protein sources. In this study, we focus on the digestion of canola seeds protein gels. Canola (*Brassica napus*) is considered to be a very good source of high-quality proteins, positioned above many other plant proteins and even comparable with quality of proteins in milk or egg[30,31,32]. A high content of essential amino acids, together with a nutritional compatibility and a functional suitability give canola proteins a great biological value and a high potential for use in human nutrition[31, 32, 33, 33].

Our interest is to study (i) the effect of the structure of the model protein foods (heat-set canola gels prepared at different pH values) on the kinetics of *in vitro* gastric and intestinal digestion processes, and (ii) the effect of the two digestion steps on the structural evolutions of the gels.

We used Small-Angle Neutron Scattering and oscillatory rheometry to obtain structural information on the digestion mechanisms at the nanometric scales and the macroscopic mechanical behaviour at different time scales, respectively. It is worth mentioning that, even though there are studies on the overall protein structure using the above-mentioned techniques, works on protein structure under gastro-intestinal digestion are rare[34,35]. However, a few more authors dedicated their works in the digestion field not to proteins but lipids[36,37,38]. Note that the dimensions of the samples (10 to 15 mm in diameter, 1 mm in thickness) investigated in SANS and rheology were similar, and close to the ones of a real food particle. In each experiment, we approached to achieve a homogeneous enzymatic distribution inside the whole volume of the sample, prior to performing digestion. That being said, our methodology and experimental techniques to study protein structure under *in situ* and *in vitro* gastro-intestinal digestion are original while challenging choices.

A former paper from our group has examined the SANS from similar canola protein gels[39]. The essential differences are: (i) much more advanced and extended analysis of the SANS data, with a more detailed description, highlighted by data presentation in $q^2 I(q) \, versus \, q$,, (ii) a larger range and number of investigated gastric and intestinal digestion times, (iii) the rheological measurements of the same types of gels as for SANS, in similar digestion

conditions. Moreover, the control level of the experiments made us able here to correlate different behaviors in SANS and rheology to the different structure of the gels obtained by varying pH.

Materials and Methods

2.1. Proteins

The canola protein isolate was obtained from Teutexx Proteins (Oakville, Canada) by W. N. Ainis. The isolate was reported to have a protein content of 92%, together with 6% moisture, 1% ash and 0.6% fat, and traces of phenolic compounds[40]. It consists of a mixture of two most abundant canola seed storage proteins, cruciferin (12S globulin) and napin (2S albumin), in proportions of about 54% and 46%, respectively. These two proteins differ from each other by their molecular weights and their IEP values. Cruciferin is a hexamer (~300 kDa), containing an α-(acidic) and a β-(basic) chain in each unit, giving the IEP of the molecule in the neutral pH ~7 [41,42] (other authors reported however different IEP values in the pH range from 4 to 8 [43,44]). In comparison, napin is much smaller (~14 kDa) and basic, 2-chain protein, with the IEP at the pH ~11[38,45,46]. In our own zeta-potential measurements, we found the IEP of cruciferin and napin in 10 mM NaCl buffer solutions, at the pH of 3.8 and 9.8, respectively (**Fig. SI. 1**). Note that IEP cannot be measured in solutions with higher protein and NaCl concentrations, since it is above the limit for the zeta potential measurements.

An advantageous point of using this protein isolate was the fact that both napin and cruciferin conserved their native conformations when in solutions, i.e., they were not denatured by the exctraction and purification processes, as verified by accurate Small Angle X-ray Scattering (SAXS) measurements (**Fig. SI. 2**). This permitted us to verify the effect of a heat processing on the proteins' resistivity and, finally, to follow the conformational changes of the proteins in digestive conditions on the native-like proteins.

2.2. Enzyme and reagents sources

Pepsin from porcine gastric mucosa (lyophilized powder, 3200-4500 U/mg protein), pancreatin from porcine pancreas (P1750-100G; 4 x USP specifications activity), porcine bile extract (0.93 mM of bilar salts per g of bile) and all other chemicals used in this study were of analytical grade and were purchased from Sigma-Aldrich, Inc. (St. Louis, USA.). The enzymes and bile were stored at -20 °C. Milli-Q water (resistivity 18.2 MΩ cm at 25 °C, Purelab ultra, ELGA) was used in all sample preparation steps.

2.3. Preparation of canola protein solutions and gels in initial stage

Canola protein isolate powder was dispersed in Milli-Q water containing 85 mM NaCl and 15 mM NaN_3 (the later for protein stabilization and against bacterial growth, respectively) to reach the desired protein concentration of 100 g/L. The dispersion was then allowed to solubilize by a gentle stirring overnight at the room temperature, to ensure a complete dissolution of the powder. The obtained protein solution was subsequently centrifuged (Centrifuge 5810r, Eppendorf) at 10.000 rpm for 20 min at 20 °C and the collected supernatant was centrifuged once again under the same conditions. From the final supernatant, two aliquots were prepared – adjusted to pH 8 and to pH 11 with either 0.5 M HCl or 1 M NaOH. The final concentration was verified by the UV absorbance at 280 nm of the diluted protein solution. The molar extinction coefficients were 14480 $M^{-1}.cm^{-1}$ for napin and 42650 $M^{-1}.cm^{-1}$ for cruciferin.

2.3.1. Preparation of gels for rheometry

In order to induce gelation, 2 mL of the protein solutions was transferred into sealed Luer Lock syringes with diameters of 13 mm and immersed upright in an oven/water bath regulated at 95 °C for 30 min. During the first 5 min of the heating, the syringes were rapidly but gently tapped, in order to remove air bubbles from the volume of solutions. After the heating, the formed gels were let cool down at the room temperature for 30 min and stored at 4 °C up to one week, prior to use. The protein solutions changed colors to lighter ones during the thermal processing, already suggesting structural modifications during the gelation.

2.3.2. Preparation of gels for SANS

The main features of the preparation protocol are the same as for rheometry, only with several specificities. The solutions were poured first into syringes, then in following sets of experiments either into flat neutron cells (diameter 15 mm, in 1 mm or 2 mm thick), or in Eppendorf tubes (1.5 mL) and cooked in a water bath/oven at 95 °C for 30 min. The solution appeared gelled, with a small amount of supernatant (< 0.2 mm height).

2. 4. Preparation of simulated digestion solutions

The simplified methodology of the protein digestion and preparation of the simulated digestive reagents were based on the standardized INFOGEST protocol[47,48] and followed through all experiments. The function of the simulated gastric fluid (SGF) and the simulated intestinal fluid (SIF) was to mimic the composition and environment of the human gastric and intestinal juices, and at the same time, by being less complex, to be easier to control and thus

possible to achieve in our experiments. The amounts of enzymes added in each digestion phase were based on their specific activities and calculated for the total volume of the digestion mixture (i.e. the gel sample plus the digestive juice). The ratio of the gel sample to a simulated digestive juice in the total digestive mixture were 1:1 (vol:vol). This rule was applied for the rheometry and the first sets of SANS experiments, while in their second part, the gel pieces were soaked in a large excess (factor 100) of the digestive juice.

2. 4. 1. Simulated gastric fluid

The SGF was composed of pepsin (diluted to 2000 U mL^{-1} in final mixture), water and 0.01 M hydrochloric acid, to give the final pH of the gastric mixture between 2.0 and 2.3. The initial activity of porcine pepsin was found to be of 3564 U/mg of protein, measured by a standardized assay as trichloroacetic acid (TCA)-soluble products and using haemoglobin as a substrate. Before each gastric digestion experiment, a fresh pepsin stock solution was prepared and stored on ice for maximum 2 h before being used for the digestion experiment.

2. 4. 2. Simulated intestinal fluid

The SIF was composed of pancreatin (at 100 U mL^{-1}), bile (at 10 mM), water and sodium bicarbonate (0.1 and 1 M), required to neutralize the mixture to pH 7. Pancreatin is a mixture of several digestive enzymes produced by the exocrine cells of pancreas. It is mainly composed of an amylase, lipases, and proteases (primarily trypsin and chymotrypsin), allowing to hydrolyze starch, fats and proteins, respectively. The choice to use the pancreatic mixture instead of individual proteases was guided by the facility to use all proteases (mainly trypsin, chymotrypsin, elastase) at once. The theoretical activity of trypsin was of 100 U mL^{-1}.

A 1600 U mL^{-1} (228.6 mg/mL) mother solution of pancreatin was prepared by magnetic stirring in cold room (4 °C) for minimum 30 min, until a complete solubilization of the enzymes, except for mucous lumps which were removed, if appeared. After two successive centrifugations (10.000 rpm, 20 min, 4 °C), the final supernatant was recovered and stored at 4 °C for a maximum one day, or frozen at – 20 °C.

Bile is an alkaline fluid produced by liver and consists of, i.a., bile salts, made of bile acids conjugated with glycine or taurine[49]. Its general function is to help in lipid digestion by emulsifying fats, enabling lipase to further break them into fatty acids[50]. Due to their amphiphilic character, they may also act on proteins. Indeed, the conjugated bile acids were found to enhance the protein digestion by accelerating their hydrolysis by proteases from pancreas[51].

7

A 172 g L^{-1} bile stock solution was prepared by strong magnetic stirring in a cold room (4 °C) for minimum 30 min. After two successive centrifugations (10.000 rpm, 20 min, 18 °C), the supernatant was recovered and stored at 4 °C for one day maximum, or frozen at – 20 °C.

2.5. In-vitro and in-situ digestion procedures

The food digestion *in vivo* includes the exposure of the food to three successive phases, i.e. oral, gastric and intestinal. According to the INFOGEST protocol[47,48], the oral digestion (mechanical and chemical) is an optional step, not required in case of proteins, due to absence of proteases in the saliva. It is however recommended for the food sample to be of a real-size bolus, possible to swallow *in vivo*. In our study, the gel samples dimensions (Ø 10-15mm, thickness 1-3 mm for rheology and SANS, respectively) were small enough to neglect the mastication step. For both gastric and intestinal phases, a static digestion model was used, where the experimental conditions were kept constant (temperature, enzyme concentration, pH) and no agitation was applied.

2. 5. 1. In-situ digestion on rheometer

Rheological measurements were carried out, in order to monitor the structural changes in the canola protein gels produced at two different pHs during the gastric and intestinal digestion.

The initial states of the gels were always determined before the digestion experiments: the cylindrical protein gel was cut with a razor blade to obtain slices of approximately 3 mm. One slice was then put down on the lower plate of the rheometer's measuring system and then carefully compressed in the normal direction by moving the upper plate downwards. Because the gel slices were never identically cut, the gap width was varying with the sample thickness, around the value of 2 mm. Based on the visual aspect of the sample and the normal force, controlled when closing the gap and compressing the gel, the accurate value of the gap width was chosen so that the gel was sufficiently compressed without being damaged (i.e., a slight bulge on the edge between the sample and the plates was observed, together with a detection of slight increase in the normal force (< 0.1 N), signaling a contact with the sample, without syneresis). Subsequently, the sample was allowed to equilibrate at 37 °C for 2 min and the rheological tests started (cf. 2.6 for detail about rheometry).

Prior to the digestion experiments, the temperature on the rheometer was lowered to 4 °C and then the gel slice was immersed in the enzyme solution with a pH away from its optimal activity. Such an inactive enzyme was then allowed to diffuse through the gel sample and distribute itself through its whole volume without starting the hydrolysis.

For the gastric digestion, the sample was kept in such conditions for 1 hour, after which the HCl was added, lowering the gastric solution to pH ~2. After 15 min of the acid diffusion to the sample (being in principle much faster than diffusion of the enzyme), the solution surrounding the sample was removed and the upper measuring plate gently put in contact with the gel, as described above. The temperature was then raised to 37 °C in a few minutes, activating the enzyme and initiating the digestion at the beginning of the first measurement. Such an approach enabled us monitoring the structural changes *in situ*.

For the subsequent intestinal digestion, the temperature was once again lowered to 4 °C and the pre-digested sample was immersed into the $NaHCO_3$ solution, raising the pH to 5 (able to inactivate pepsin[24] without the acid denaturation of the upcoming pancreatin). The enzymatic mix was then added to the solution and allowed to diffuse in cold for 30 min (shorter time than for gastric digestion, due to the necessity of being at pH not completely deactivating trypsin, therefore with a risk of starting the digestion before running the measurement). At the end of diffusion, the pH was increased to the optimal value of 7. The sample was put in contact with the measuring plates, the temperature reached 37 °C and the rheological measurements *in situ* started. The gap width remained constant during each whole set of a digestion kinetics experiment (with the same slice of the gel).

Some gel samples were also incubated with SGF or SIF without the enzymes, in order to estimate the individual effect of $HCl/NaHCO_3$.

To prevent samples from drying during the experiment, a thin layer of paraffin oil was applied on the edge of the geometry and a cotton tissue, soaked with distilled water, was placed around the sample, to maintain water-saturated atmosphere at its edges.

2.5.2. In-vitro digestion for SANS

Gel slices were obtained depending upon the used gelation container: neutron cells, syringes or Eppendorfs; the two latter were cut through and the gels were pushed out and cut in slices of 2.5 +/-0.5 mm. As previously mentioned, the gels for rheological measurements were soaked in a volume of the juice adjusted to the volume of the gel. For SANS, the protocol varied: the slices were introduced to an excess of the 2000 U mL^{-1} pepsin solution in a Falcon centrifugation tube. In our former work[39], « Mel » gels – also shown here (cf. 3.3.3.) - were mixed with only the necessary amount of pepsin delivered in small volume added amounts. The tube was immersed in an ice bath (0 °C) for 1 h, to give enough time for the gel

penetration by pepsin. HCl was then added to reach a pH between 2 and 2.3, and the tube was kept for a minimum 10 min at 0 °C.

The gel slices were removed from the tube for the time of its preheating to 37 °C and then they were placed back into the tube for a chosen gastric digestion time t_{GAS} (between 10 min and 2.5 h), at 37 °C. Swelling of the gel pieces was often observed after typically 15 min, resulting in more transparent slices, while in parallel, a slight decrease in mass could be inferred. For each t_{GAS}, one or several slices (enough to fill a 10-12 mm diameter, 1 mm thick SANS cell) were used to be analysed.

For the subsequent intestinal digestion, performed after t_{GAS} = 15 or 30 min, some gel slices were permeated by the pancreatic enzyme solution at pH 7, in a tube placed in an ice bath for 1 hour (like in the gastric step, to give enough time for the enzymes to penetrate homogeneously without their activation). Afterwards, the digestion was performed at 37 °C for a chosen intestinal digestion time t_{INT} (between 10 min and 2.5 h), before quenching at 0 °C. Onset of the digestion, resulting in a decrease in size, was visible after a few min - much faster than in the gastric digestion. The gel slices were then introduced to the neutron cell and quickly transferred on the sample changer of the spectrometer thermalized at 4 °C.

2.6. Rheometry measurements

The viscoelastic moduli G' (elastic) and G'' (viscous) were measured using a Modular Compact Rheometer MCR 302 (Anton Paar GmbH, Austria) equipped with a thermal stabilization comprising a Peltier element and a temperature control bath, together with a temperature bonnet fed by heated air. We used the stainless-steel parallel plate geometry with Ø 15 mm and a profiled surface (PP15/P3, Anton Paar).

Preliminary strain sweep tests, carried out in a strain range from 0.01% to 10%, at angular frequency of 1 Hz (6.3 rad.s^{-1}) and at fixed temperature of either 20 or 37°C, showed that a strain of 0.1% was within the linear viscoelastic region (LVR) for all samples. This strain value was used for all further rheological measurements.

Each angular frequency sweep test in the range from 0.1 to 250 rad.s^{-1} took ~10 min, with an interval rest time of 40 s. The tests were looped for the recommended duration of 2 h for both the gastric and the intestinal digestion. All studies were carried out at least in triplicate. Much care was taken to prevent slippage, at least in the frequency range presented in results (i.e. up to 90 rad.s^{-1}), by using measuring plates with profiled surfaces.

2.7. Small-Angle Neutron Scattering

The measurements were performed on the PAXY spectrometer at Orphée reactor - Laboratoire Léon Brillouin at CEA, Saclay. Three q-ranges were chosen: high q at 1 m, 6 Å; medium q at 3 m, 6 Å and low q at 6.7 m, 15 Å, covering a q range from 2.10^{-3} Å^{-1} to 4.10^{-1} Å^{-1}. The gel samples were placed in the middle of a spacer ring and sandwiched in between two quartz plates. Digestion was quenched by regulating the sample changer at 4 °C in dry nitrogen, owing to a temperature-regulated bonnet. External condensation on the quartz windows was avoided by a multi-jets airflow.

As indicated in 2.3.1, all the gels were prepared with using H_2O as a solvent. Therefore, the sample scattering comes from the difference in scattering length density between the H_2O and the protein molecules, which SLD corresponds to 42% D_2O/58% H_2O; there is thus a sufficient difference with the SLD (H_2O).

2D scattering profiles were radially averaged and normalized to the sample transmission and sample thickness. Corrections for the detector sensitivity, background noise and empty cell signal were applied[52]. The absolute scattering cross sections $I(q)$ per unit sample volume in cm^{-1} was obtained using normalization of 1 mm thick water cell.

The experimental scattering profiles of all the gel samples were fitted with a Two Lorentzian model available in *SasView* software[53], described by Eq. 1:

$$I(q) = \frac{A}{1+(q\xi)^n} + \frac{C}{1+(q\Xi)^m} + Bkg \qquad\qquad Eq.\ 1,$$

where the 1st term, dominating at high q range, characterizes scattering from elementary components of the gel (i.e., individual proteins), while the 2nd term, dominating at low q, characterizes the structural order and interactions between the elementary components in the gel (i.e., scattering from aggregated proteins). The fitting parameters ξ (high q) and Ξ (low q) correspond to the specific correlation lengths at two distinct scattering vectors ranges, giving estimations of the gel and mesh sizes, while the n (high q) and m (low q) exponents give indications of the gel components compaction (i.e., proteins and aggregates, respectively). The scattering intensity scaling as q^{-4} reveals compact conformations, whereas scaled as q^{-2} - unfolded ones. Parameters A and C represent the respective scale factors and Bkg - an incoherent background scattering.

Results

3.1. Visual observations

Before describing the rheometry and SANS results, we will shortly present the visual properties of the samples after gastric and intestinal digestion steps.

In the initial states, the gels appeared to be homogenous. For rheometry, gastric digestion resulted in a slight change in color to whiter (possibly suggesting increased aggregation) and a slight increase in its size, indicating the swelling conditions. For gastro-intestinal digestion, we observed progressive changes occurring at different times after in-situ digestion on the rheometer, examples are shown in Fig. S.I.4. The surface of the 20 min sample appears to be homogenous but becoming dissolved by the enzymes; after 1h some regions of slightly different colors are visible, suggesting a progressive heterogeneity; after 2h, the gel appeared to be heterogeneous, with the rims being transparent and the core still brown – the gel seemed to flow.

For SANS, we could follow the evolution during the samples preparation. In the gastric phase, the gel pieces became more transparent after 10 min, they exhibited swelling (with sizes variations by 10 to 30%, i.e., 30% to 100 % in volume). This is confirmed by UV fluorescence microscopy (to be published). In the future, we plan systematic measurements of the swelling ratio of the gel during digestion, by removing the liquid from the gel surface before weighting the gel. Finally, a decrease in size appeared, while samples nonetheless, appeared homogenous.. In the gastro-intestinal phase, the decrease in size was increasingly faster, while an external erosion appeared, in the form of more transparent and softer material at the edges. This led us to limit the intestinal digestion time to 30 min.

3.2. Rheology

Fig. 1 (corresponding to the gel at pH 8) and **Fig. 2** (corresponding to the gel at pH 11) show variations with angular frequency of the storage modulus G' (stiffness, elasticity of the material) and the loss modulus G'' (dissipated energy, viscous response)[54], at different gastric and intestinal digestion times. For both pH gels, the viscoelastic nature of the samples makes G' predominant over G'' throughout the whole range of the tested frequency (in other terms, values of $tan\ \delta = G''/G'$ were always much less than a unity). This indicates a solid-like mechanical behavior, which confirms the transformation of the protein solutions into elastic networked structures by the means of the heat treatment.

The moduli are very close to be constant for low frequencies, corresponding to longer length scales. This can be related to scales larger or equal to the mesh size of the whole network and correspond to its good connectivity[55]. Meanwhile, at high frequencies, we address the relaxation times internal to the mesh. Indeed, we observe a smooth increase of G', and a

stronger one for G'', along with the oscillation frequency ω until 50 rad.s^{-1}. The range above 50 rad. s^{-1} is however rarely addressed in most of the papers. We observe a stronger and stronger increase with ω (**Fig. SI. 3**), but the final upturn appeared to depend on the settings of the rheometer.

3.2.1. Gel formed at pH 8

In initial state (black starred symbols), G' value at 1.15 rad.s^{-1} equals 1518 Pa, being over 10 times greater than its corresponding viscous modulus G''. As said above, this confirms the transformation of the protein solutions into elastic networked structures. At higher frequencies, G'' is more frequency-dependent than G' (*tan δ* increases from 0.1 to 0.14).

After 30 min of gastric digestion (**Fig. 1**; red symbols), a slight decrease of G' and G'' over the whole frequency range is observed. Values of *tan δ* at 1 - 35 rad.s^{-1} increased similarly to the initial samples, from 0.1 to 0.13 (data not shown). The reduction in G' could be attributed to general weakening of the interactions between proteins (gel strength reduction) at the gastric pH and cutting the bonds in and/or between the protein aggregates by pepsin, resulting in their sizes reduction and/or loss of connectivity.

Fig. 3a (circles) shows the time dependence of G' and G'' at a frequency of 1.15 rad. s^{-1} during 2 h of gastric digestion. A slight decrease of the moduli is slowing down with time: after 30 min, the value of G' drops by about 10% to a value of 1360 Pa (G'' decreases by a similar fraction), while after 120 min, it reduces only to 1313 Pa. During this gastric step, *tan δ* at 1.15 rad.s^{-1} slightly increases from 0.095 to 0.105, showing not much change in the gel strength.

Intestinal digestion, after GAS 30 min step, (**Fig. 1**, dark green circles) is much more efficient, compared to the gastric one: in 1 h of its duration, the moduli decrease strongly, being a clear sign of hydrolysis, with a progressively slower rate, reaching G' of 369 Pa at 1.15 rad. s^{-1}. The frequency dependence becomes also much more pronounced (*tan δ* raising from 0.13 to 0.19 at 1.35 rad. s^{-1}), suggesting an internal deconstruction of the network.

Fig. 3b (black circles) shows a time variation of G' and G'' at the frequency of 1.15 rad. s^{-1} during intestinal digestion; G' curve is fitted with an exponential decay function having two time-constants, a fast one (6 min), and a slow one (77 min). This variation is prolonged by the values obtained via additional intestinal digestion (blue circles), i.e., first point after 1 h *in vitro* (immersing the gel sample in the SGF at 37 °C for 1 h) and continued *in situ* (placed on the rheometer at 37 °C for another hour). Fig. 3b shows a very good connection between data

of the two digestion protocols. Eventually, at 120 min, *G'* drops suddenly from 190 Pa to 72 Pa, along with a stronger frequency dependence, of both *G'* and *G"*, and an increase of *tan δ* at 1.15 rad. s^{-1} from 0.14 to 0.19, suggesting the onset of a kind of de-percolation of the gel (**Fig. SI.4**, magenta circles).

3.2.2. Gel formed at pH 11

Fig. 2 shows the evolution of $G'(\omega)$ and $G''(\omega)$ of the gel formed at pH 11 in the curse of digestion. When compared to the gel formed at pH 8, this gel exhibits initially higher values of both moduli (for *G'* precisely by 187 Pa at 1.15 rad. s^{-1}) and less frequency dependence; during digestion, both moduli of the gel were also less frequency-dependent. This finding is consistent with reports showing that canola protein gels prepared under alkaline conditions had higher *G'* compared to the gels prepared under lower pH[56,57].

During gastric digestion, strikingly, an increase in values of the viscoelastic moduli was observed – an outcome opposite to the one of the pH 8 gel. This effect was observed repeatedly. To eliminate the possibility that such behavior is an effect of the sample's drying, we performed the frequency sweep tests at 37 °C without the SGF with keeping the same time protocol. The results do not show any variation of the *G'*, *G''* (ω) curves in time (**Fig. SI. 3**). The increase of elastic response of the gel during this digestion is therefore an effect of the SGF, comprising the possible effects of the low pH and the enzyme.

The effect of HCl alone was verified on both samples: it indeed induced the enhanced elasticity, however only in the case of the pH 11 gel (**Fig. SI. 5**, red stars) and without any increase of *G'* with time. Conversely, at the first 10 min of the gastric digestion, we observe a step rise of *G'* (from 1705 to 2116 Pa at 1.15 rad. s^{-1}), together with an increase of *tan δ* (first 20 min). It is followed by a 1 h of a very smooth increase of *G'* (up to 2315 Pa) and a decrease of *tan δ*. At 70 min, a second jump of *G'* (up to 2976 Pa) occurred, along with an increase in *tan δ*. This implies that the presence of pepsin together with HCl was continuously modifying the gel structure. The improved gel strength might be due to strong acid ionization, which could enhance the protein unfolding and the subsequent protein-protein interactions, leading to stronger aggregation or formation of bigger aggregates at first. The additional work of pepsin in such environment could induce creation of a larger number per volume of smaller aggregates, leading to a larger network modulus, following the theory of rubber elasticity. Such an enhanced solid-like behavior was not observed during the gastric digestion of the pH 8 gel, maybe due to its already more unfolded structures before digestion.

By only raising the pH of the gel from 2 to 7 (intestinal pH), by addition of Na_2CO_3, an increase in G' is also observed, as after HCl addition (**Fig. SI. 5** green triangles). It can be, once again, due to an ionization, this time above the IEP of cruciferin.

During the intestinal digestion, the decreasing trend of G' is similar to the one of the pH 8 gel: in the first 10 min, the sample lowers its strength already down to 1556 Pa (by 30%, as for the pH 8 gel), and then, it continues to decrease with lower rate (like for the pH 8 gel), reaching 351 Pa after 120 min. **Fig. 3b** (triangle symbols) shows G' and G'' values as a function of intestinal digestion time at 1.15 rad. s^{-1}. The time constants of the exponential decay function obtained from the fit are of 16 min and 151 min - both longer than for the digestion of the pH 8 gel (6 min and 77 min, respectively).

The decreases of G' and G'' with intestinal digestion time were observed repeatingly on different gel pieces from the samples prepared at both pH 8 and pH 11. The results for the same digestion conditions were very reproducible.

In summary, the gel preparation pH has strong effects on the initial values of moduli, and their evolutions via the reaction to the acid gastric juice, and via the resistance to the intestinal digestion.

3.3. Small-angle neutron scattering

We present the scattering intensity, $I(q)$, using two plotting approaches. The first representation, on a double logarithmic scale $log\, I(q) - log\, q$, enables us to capture the variation over the whole q-range. However, we meet here the following difficulty: the intensity level seems to vary from one sample to another by a variable prefactor. In principle, and from our other experiences, e.g., using SAXS, the digestion of the sample should result in decreasing of its scattering intensity. The discrepancy from this feature, sometimes observed in this study, could be explained by a poor control of the volume of the gel inside the neutron cell. More precisely, in the course of digestion, the gel piece became smaller than the neutron cell volume, corresponding to the beam cross-section, and thus, to overcome this issue, more sample pieces were brought together to fill the neutron cell. This could sometimes result in their squeezing and lead to deswelling (increasing concentration). The differences in scattering intensities can thus be a matter of differences in protein concentrations. Finally, the gel swelling may evolve with time inside the neutron cell. That could lead to drifting of the gel, or some of its pieces, in part, out of the beam. Deswelling, or swelling, are other possible origins of a poor gel volume control. Such dissimilarities concern the prefactor, but they do not affect neither of the curve's parameters which determine its shape (i.e., slope and

correlation length). Note that, to be better visualized on the plots common with other curves, the scattering intensities for some digested samples were divided by factor F = 1.5, or higher.

The second representation, $q^2 I(q)\ vs\ q$, (the Kratky plot), enables to visualize more accurately the large q behavior, corresponding to the scale range of individual proteins. This plot is very sensitive to their size, compacity/unfolding and possible interpenetration. Since this representation is focused on the allure of the curves, we did not use the correction factor F, which also enables us to keep track of the real scattering values.

Furthermore, to follow the size and shape variations more easily, we have also fitted the data to the double-power law function presented in Materials and Methods (Eq. 1). Results are listed in **Table 1**.

3.3.1. Samples in initial states

Log-log plots. **Fig. 4** presents the scattering profiles from the two studied canola protein gels, at pH 8 and pH 11.

At low q, below 0.01 Å⁻¹, both spectra display a strong upturn in intensity towards lower q values, with a power law exponent of 4. Such a well-marked contribution is not present in protein solutions, before gelling, as shown earlier[39]. It usually indicates attractive inter-particle interactions, while the large value of the exponents, close to 4, reveals a rather strong protein aggregation, or a partial phase separation between regions poor and rich in proteins during the heat-treatment. We notice a higher intensity contribution of the scattering from the pH 11 gel. Note that the visual observations also revealed that the pH 11 gel scatters light more than the pH 8 gel. However, it is not possible to conclude whether it is due to a bigger fraction Φ_{agg} of aggregates of a given size or to a bigger size D_{agg} of aggregates - the two quantities contributing as a product to the prefactor of the power law. This remark holds in the following for the decrease of the low q signal, which we will interpret by the term "degradation or coalescence" of the aggregates.

At large q, above 0.02 Å⁻¹, after the slight decrease, a rather well-defined shoulder appears in the scattering spectrum of the pH 11 gel. It is a characteristic of the form factor of a folded protein conformation, being here the compact, toroidal shape of cruciferin (which, owing it to its high molecular weight, dominates over the scattering of the small napin). For the pH 8 gel, such form factor oscillations in the scattering are less visible.

Kratky plots. The differences in conformation states of individual proteins can be seen more clearly in the Kratky plot shown in the inset of **Fig. 4**. The high q scattering from completely unfolded proteins (Gaussian chains) approximates to $1/q^2$, giving a plateau in the Kratky plot,

while the scattering from folded (compact) objects goes as $1/q^4$, giving hence a maximum followed by a decrease in the Kratky plot.

Indeed, in **Fig. 4**, while the $log\ I(q) - log\ q$ shows a slope of -3.2, a well-defined peak in $q^2I(q)$ is visible for the pH 11 gel (inset of **Fig. 4**); this indicates a predominance of compact/folded protein conformations in this gel. Conversely, for the pH 8 gel, the scattering at higher q decays more slowly, with the slope of -2.3 (broad peak), such that $q^2I(q)$ shows a plateau at high q. This indicates relatively unfolded protein conformations for the pH 8 gel. The comparison of scattering from canola protein solutions and corresponding gels were presented in ref. [39], where a similar lack of intensity oscillations in high q region was noted for both the solutions and the gels at pH 6 and 9. The majority of canola proteins in our pH 8 solution before the heat-treatment seemed already more unfolded due to the pH, comparing to the proteins at pH 11 with more compact conformations. Nevertheless, neither of the gels are described by an ideal bell-shaped Kratky plot (native protein) nor by a full plateau at large q (completely unfolded). This indicates that proteins in the gel networks are in intermediate situation, retaining partly their levels of compactness, or that they have different level of unfolding.

From the relative positions of the intensity maxima on the Kratky plots, the difference in sizes of the probed objects can also be deduced. Although the pH 11 gel exhibits more local compaction, its peak is located at lower q, and its correlation length ξ is slightly larger (27 Å), in respect to the pH 8 gel (25 Å). The local components of the pH 11 gel could be, in fact, made up of a few proteins, seen as both bigger and more compact.

3.3.2. Gastric and gastro-intestinal digestion

Before studying the effect of the digestive enzymes, we can first check the effect of the low pH due to the HCl addition in the gastric digestion. **Fig. SI. 6** shows a small shift of the curves for the pH 11 gel towards lower q values by a translation factor 1.2, suggesting an increase of all "sizes" by a factor 1.2, which would correspond to a swelling of the aggregates by 70%. We did not see such a result for the napin or cruciferin gels prepared at pH 8 (data not shown). Concerning the low q range, there is no strong increase of the scattering, differently from the acid-induced aggregation/phase separation effect observed formerly after the HCl addition to the protein solutions[39]. The gel structure has thus a stabilizing effect.

Fig. 5 shows changes in structures of the pH 8 gel, occurring after short (30 min) and long (120 min) gastric digestion steps. The overall shape of the initial scattering profile changes visibly. The upturn at low q, much visible in the initial state, is slighter (but still present) after

the short and the long gastric phase, indicating a primary but not complete degradation or coalescence of the aggregates by the SGF. We do not observe any well-defined lower exponent as would produce the presence of a gel network of a lower fractal dimension (e.g., a power law with exponent around 2). The aggregates are likely to stay compact.

At high q, the evolution is subtle, which is better seen on the $q^2 I(q)$ representation (inset of **Fig. 5**). While the initial pH 8 gel presents a broad shoulder, approaching a plateau at large q, after 30 min of gastric digestion, a bump appears at slightly lower q, suggesting a slight compaction, combined with possible local protein aggregation. This is shown in by the fitting parameters (Table 1): the high q exponent increases slightly (compaction) but ξ increases more significantly during those 30 min of the gastric digestion, namely from 25 Å to ~ 31 Å.

For the 120 min gastric step (**Fig. 5**), at large q, the Kratky curve's peak shifts back towards the higher q values, together with a smaller exponent. The evolution of the structures seems to reverse back to the initial unfolded state: the intermediate aggregates appear to be suppressed and smaller unfolded structures to be created.

In addition, **Fig. SI. 7** shows how the scattering of the pH 8 gel is evolving for 15, 30 and 45 min of gastric digestion, being complementary to Fig. 5. We can see a decrease of a low q signal and a slight curve's bump flattening from 15 to 45 min, indicating a progressive aggregates dissociation or coalescence, and a tendency to protein unfolding, respectively. Moreover, a slightly stronger shift of the Kratky plots' peak towards lower q, for GAS 15 min than for GAS 30 min (inset of Fig. SI. 7), indicates stronger local aggregation at the beginning of the digestion. A progressive tendency of the correlation length increase until observed 45 min of digestion can be visible from the left-handed side of the bump of the curves. Although we are lacking SANS data between 45 and 120 min of digestion, we assume that during this time period the unfolded proteins started to decrease in size.

10 min of intestinal digestion, applied after 30 min of gastric digestion, clearly strengthens the trend observed for the latter, as seen in **Fig. 7** (the same as after only 15 min of gastric digestion in **Fig. SI. 8**): a more pronounced bump at much lower q suggests further compaction, combined with possible further local protein aggregation, respectively. This is the opposite from letting gastric digestion act 90 min more.

The general evolution of the pH 11 gel (**Fig. 6**) resembles, only partly, the one of the pH 8 gel. After 30 min of gastric digestion, the low q upturn is neatly reduced but this is reversed in the GAS 150 min sample (while the intensity factor is noticeably decreased). For GAS 30 min, at large q, the Kratky plot shows a widening of the bell-shaped curve, observed for the initial sample. The shift towards lower q is not very pronounced for this gel. These features

are slightly reversed in the GAS 150 min sample. **Fig. SI. 9** confirms satisfyingly these trends for GAS 15 min and GAS 45 min, as in the case of the pH 8 gels.

For the intestinal digestion step, a more pronounced bump, and its slight shift towards higher q (compared to the gastric step) are observed (inset of **Fig. 8**). These features reveal smaller protein structures and their stronger compaction. However, since the proteins in this gel come from less unfolded structures after GAS 30 min, this re-compaction is thus softer than for the pH 8 gel.

Note that recently we performed more detailed SAXS measurements (to be published) which clearly confirm the trends observed here. Altogether, with SI Figures, we have a consistent set of data.

3.3.3. Other gels

Measurements for gels of another mixture of cruciferin (35%) and napin (29%), filtered by size exclusion chromatography, and noted « Mel »[39], exhibited initial scattering very close to the gel presented so far. For Mel prepared at pH 9, close to our pH 8 gel, we also observe (i) the shift of the Kratky plot maximum towards lower q, (ii) the reduction of the low q signal at short gastric digestion and (iii) the high q compaction for the intestinal digestion (**Fig. SI. 10**). For Mel prepared at pH 11 (**Fig. SI. 11**), we confirm the compaction occurring under the intestinal digestion.

3.3.4. The ξ, n diagram

Trends can be seen also on the ξ, n diagram (**Fig. 9**), displaying correlation lengths and exponents at high q given in Table 1. The arrows show the direction of the protein's evolution during gastric (red) and intestinal (green) digestion. A consistent picture for the two pH gels arises from this diagram. To summarize rapidly, a half-loop is observed from the left to the right and back from the right to the left: the correlation length increases during the first gastric digestion step, after which the evolution is reversed at longest times. For the pH 11 gel, the exponent decreases a lot and gradually, while for the pH 8 one, it varies only slightly, firstly increasing, then reducing back and increasing again. The differences between the two gels are due to the initial states of their proteins. To reach the smallest objects, it takes a long time for two different reasons: for the pH 11 gel, because of a long process of protein unfolding, and for the pH 8 gel – because of the formation of intermediate aggregates from already unfolded proteins.

Intestinal digestion provokes a rapid shift to lower ξ and increase of the exponents for both gels, which can result mostly from contraction but perhaps also from the protein scission. This is at variance with the decrease of ξ values for the longest gastric digestions, which origins probably mainly from cutting of the unfolded proteins.

To roughly conclude, gastric digestion ends with rather unfolded and smaller protein parts, while gastro-intestinal digestion leaves small but rather compact pieces.

4. Discussion

For both rheology and scattering, the evolution of the occurring processes is complex and, in part, unexpected, in particular for the gastric digestion. The main results are however easy to summarize. For both techniques, the characteristic profiles remain similar. *G'* and *G''* versus ω during digestion indicate a continuous softening of the gel, which shows a decreasing crosslinking density but still remaining a connected net. The scattering profiles still display low q and large q contributions, indicating the presence of the aggregated network and individual proteins, respectively.

4.1. Initial states: effect of preparation pH

For the initial pH 11 gel, the large q SANS shows a scattering close to the one of the native solution, while a low q scattering appears. Although native proteins are charged, the repulsive forces were not counter-balancing the hydrophobic interactions induced by the heat treatment and thus protein aggregation occurred. The observed q^{-4} behavior can be attributed to some compact aggregates and not to fractal ones. This favors the option 2 in the **Fig. 10**, inspired by the review of T. Nicolai[58].

In initial state, the profile of *G'* with angular frequency ω is a characteristic of a fully crosslinked network, much above the gelation point. It is essentially flat, as reported also for other protein gels[59], with no clear increase at large ω. However, an increase at larger frequencies (similarly to the well-known profile for polymer solutions) was also reported[60]. For *G''*, we observe a very slight increase for low ω values tending towards zero, which could signal a relaxation of characteristic time (τ_{rheo} > 10 sec).

At the pH 8, cruciferin is closer to its zero charge, as we found it by zetametry at the value of 3.8 (4.7 in reference [61]). At this pH, the protein's residues have lower net charges and the repulsion between them decreases, potentially promoting their unfolding with exposure of hydrophobic groups and polar side chains, available then for inter-molecular interactions and hydrogen bonding, respectively. Indeed, the large q scattering corresponds to the vanishing of

the oscillation related to a compact cruciferin's shape, and a smoother variation with an exponent close to 2 (as evidenced by the Kratky plot, in which the maximum is replaced by a plateau). It would be possible, since at pH 8 cruciferin and napin carry opposite electric charges, that they additionally interact through columbic attraction, however this is not seen clearly. More non-covalent interactions between the proteins can lead to aggregates formation and a further increase in their sizes through hydrophobic interactions[62,63,64].

In this pH 8 sample, the low q scattering is less intense but still shows a q^{-4} behavior, indicating existence of compact aggregates, as for the pH 11 gel. As said above, the low q intensity is difficult to interpret. In terms of the Porod scattering, it could be due to an increase in size R_{agg}, shifting the upturn towards $q = 0$, or inversely to smaller concentrations at constant (or even smaller) R_{agg}. Similarly, differences between the gel at pH 8 and 11 have been reported in recent microstructure study using Confocal Laser Scanning Microscopy[62]. It showed that canola proteins at pH 7 created thinner protein network structure (less rough, i.e., smaller aggregates, at least at the 10 µm scale), compared to those formed at pH 9. The lower value of G' for the pH 8 gel, compared to the pH 11 one, could suggest a correlation of G' to the aggregate sizes. However, it could also be due to a different crosslinking between proteins, resulting from differences in interactions as a function of ionic strength. As already mentioned, due to closer proximity to the IEP of cruciferin, the proteins at pH 8 can be less stabilized by the electrostatic repulsion, favouring unfolding and attraction of the molecules. Moreover, at this pH (being below the IEP of napin at 9.8), some additional electrostatic interactions between the two proteins can occur. In a study on the pH effect on whey protein gels, an increase of the pH above the IEP towards the proteins negative charge resulted in an increase of the strength of the gel network[65]. In our case, at pH 11, both cruciferin and napin are above their IEPs, which can explain the higher moduli of this gel.

4.2. Gastric digestion

Under gastric digestion, the $G'(\omega)$ profiles do not largely change (**Fig. 1** and **Fig. 2**). For the gel prepared at pH 8, a variation of G' is better seen with time, at a fixed ω (**Fig. 3a**): it is a decrease, as expected for a degradation of a gel upon digestion, but a very limited one. The changes in scattering (**Fig. 5**) indicate a diminishing of the large aggregates signal, but at high q (clearly visible via the Kratky plots) we observe an increase of compacity via the reappearance of a maximum in $q^2 I(q)$, strongly shifted towards lower q. Proteins, rather unfolded in the initial pH 8 gel, seem to reform more compact domains, larger than the size of individual proteins, or the correlation length of the unfolded proteins. This change of compaction cannot be explained by the lone effect of HCl since we did not observe any

conformation changes of pH 8 gels of neither cruciferin nor napin upon HCL addition. The compaction observed here must therefore result from the enzymatic attack. The protein compaction (if occurring along with the proteins staying connected to each other) should result in an enhancement of the modulus, however it is not observed here. Possibly the only slight decrease of G' in digestion time could occur due to a compensation between aggregates degradation or coalescence (seen in low q) and a local compaction (seen in high q).

Conversely, for the gel preparation at pH 11, the time variation of $G'(\omega)$ at a fixed ω (**Fig. 3a**) is a marked increase, unexpected, and comprising two successive steps. Having verified that it is not a result of drying of the sample, two possible reasons could be thought of. First, when going down to the gastric pH from pH 11, both component proteins of the gel (i.e., cruciferin and napin) are likely to cross their IEPs, making it (the gel), for that reason, more affected by the acid addition than the pH 8 one. However, the swelling by 70%, observed after adding HCl to the pH 11 gel, can hardly explain an increase of the modulus. Second, when the proteins are in almost folded states, as in the pH 11 gel, the enzymatic action can modify the electric charge and induce the unfolding of the molecules, leading to increased number of interactions (repulsion, small aggregates formation, etc.) and possible higher crosslinking, which would increase the gel modulus. Indeed, in presence of the enzyme, at t_{GAS} = 30 min, we see the enlargement of the $q^2 I(q)$, signalling both an unfolding and a local aggregation of the proteins. These processes continue at longer times.

Besides, the structure of the aggregates can also influence the process of digestion: more compact ones will hinder the access of the enzymes and slow down their dissociation. This can be the case for the pH 11 gel. Indeed, by comparing the low q scattering in **Fig. 5 and 6**, we can assume that the aggregates in the pH 11 gel are more resistant than the ones in the pH 8 gel.

Additionally, in a longer digestion process, protein parts, released from the cut aggregates, have more time to progressively re-form into local aggregates. This process can explain the second increase in G' for the more compact pH 11 gel. Finally, all along the performed duration of digestion, the processes increasing the modulus are dominating over the degradation of this gel.

To sum up, the modulus is not directly, or not only, linked to the existence and connection of the aggregates; it can be impacted also by local changes, like here - progressive unfolding and local aggregation.

4.3. Intestinal digestion

Intestinal digestion worked faster and more intensely, compared to the gastric digestion. The decrease of the moduli, seen for both preparation pHs (**Fig. 3 b**), was a more expected one. The couples of the two relaxation times (t_1, t_2) show a longer process for pH 11 than for pH 8, in agreement with the kinetics in gastric digestion. The profile G' vs ω is similar at the beginning, while, at the largest digestion time, a stronger dependency on ω is clear. For G', it is a constant decrease, at both low and large ω. This can be a signature of a deconstruction of the network, possibly due to a destruction of the initial links: between either aggregates, individual proteins, or residues inside the proteins.

For both preparation pHs, SANS show a local re-compaction, resulting probably from a change of cruciferin conformations when crossing its IEP (going up from pH 2 to 7). The proteins of the pH 11 gel stay more compact, compared to the ones of the pH 8 gel, since they were less unfolded after 30 min of gastric digestion. This level of compaction is clearly influencing the kinetics of the intestinal digestion. For the pH 8 gel, a decrease in size is seen already after 15 min. Meanwhile, for the more compact pH 11 gel, not much change at the local scale is observed throughout 30 min: as already mentioned, the enzymatic action is slowed down in denser gel structures.

Effect of compaction, if occurring together with disconnection of the proteins/protein parts involved in the network, could explain the decreasing of G' during the intestinal digestion. However, the enzymatic hydrolysis could result in some external erosion of the gel, not seen in the centre of the sample observed by SANS. This erosion would come from the fact that the residues on the borders of the gel escape from it more easily than the ones in its middle part. A resulting inherent gradient of concentration would further affect the kinetics of the enzymatic degradation, i.e., more rapid digestion on the borders. This erosion effect would be even more pronounced if the residues, staying for a long time in the middle of the gel, created additional interactions, which would further hinder the enzymatic diffusion and reaction.

5. Summary and conclusion

In this paper, we have studied in parallel the evolutions of rheological properties (oscillatory) and nanostructures (small angle scattering) of canola seed protein gels, containing cruciferin and napin. The studied samples were of about ten millimeters dimension, aiming at mimicking, as much as possible, conditions of the human digestion. We focused on the gastric and intestinal digestions of gels prepared either at pH 8 or at pH 11.

Initial nanometric structure and elastic moduli of the gels prepared at two different pHs varied from each other: rather unfolded structures of the pH 8 created a softer, but clearly networked gel, while the folded and compact conformations of the pH 11 (resembling the native structures) built a stronger network. These outcoming microstructures could be related to the proximity of the preparation pH to the IEP.

Dependently on the initial states of the gels, some rheological behaviors and nanometric structures evolutions under gastric and intestinal digestions were surprising.

Particularly throughout the gastric phase, as opposite to the slight continuous decrease of moduli and the local aggregation for the pH 8 gel, we have observed an unexpected increase of the moduli and unfolding of the nanostructures for the pH 11 gel.

We have tempted to relate these opposite rheological effects by the competition between the unfolding, which increases the interactions (and thus the modulus), and the enzymatic scission, which lowers the gel elasticity. The scission is less efficient for gels with higher network density, by likely hindering the enzymatic diffusion. Besides, some additional interactions can result from crossing the protein zero-charge point in low gastric pH (of both component proteins in case of the pH 11 gel). The balance stood out to be an increase of *G'* for pH 11 and its decrease for pH 8.

In the intestinal digestion step, differences in the behavior of the two gels tended to attenuate. When increasing the pH from gastric to intestinal (from 2 to 7), proteins in both gels were subjected to compaction. A progressive and rapid loss of moduli was observed, indicating loss of connectivity at larger size. For larger times, intestinal digestion provokes some apparent erosion of the gel. Since it is mainly localized on the external part, its influence maybe larger on the rheology, which involves the largest times, than on the scattering, which involves the centre part of the gel piece. That could explain the rather limited changes observed by SANS, in particular at low *q*.

Evidently, the digestion process imposed to the samples was not the natural one, where the food pieces are simultaneously permeated and attacked by the constantly renewed enzymes, and where the pH propagation is also progressive, in particular due to the buffer effect of proteins. We have recently tackled these conditions using deep UV fluorescence imaging but for gel pieces of several tens of microns[26]. In order to better describe the structure of the gels under digestion, we have also undertaken kinetics experiments using SAXS, in which enzymes were let diffused through mm-size gel pieces. Although the digestion conditions

were not the same as the ones described in this work, we believe that some features of the gel nanostructures evolutions will be comparable.

Acknowledgments

Figures captions

Fig. 1. Frequency sweep tests on the canola protein gel at pH 8 (100 g/L) during the digestion process at 37 °C: storage moduli (*G'*, closed symbols) and loss moduli (*G''*, open symbols) as a function of oscillating frequency (0.1-50 rad/s). The arrows indicate the direction of the digestion: 1st step – from initial gel (black stars) to 30' of gastric digestion (red squares), 2nd step – intestinal digestion kinetics during 60' (t_0 – yellow circles, t_{60} – violet circles); duration of one sweep was ~10 min.

Fig. 2. Frequency sweep tests on the canola protein gel at pH 11 (100 g/L) during the digestion process at 37 °C: storage moduli (*G'*, closed symbols) and loss moduli (*G''*, open symbols) as a function of oscillating frequency (0.1-50 rad/s. The arrows indicate the direction of the digestion: 1st step – from initial gel (black stars) to 30 min of gastric digestion (red squares), 2nd step – intestinal digestion kinetics during 60 min (t_0 – yellow circles, t_{60} – violet circles); duration of one sweep was ~10 min.

Fig. 3 a. Variations of *G'* (closed symbols) and *G''* (open symbols) at a frequency of 1.15 rad/s as function of gastric digestion time. Round symbols - pH 8; triangles - pH 11. Inset: close-up on variations of *G''*.

Fig. 3 b. Variations of *G'* (closed symbols) and *G''* (open symbols) at frequency of 1.15 rad/s as function of intestinal digestion time. Round symbols - pH 8; triangles - pH 11. Blue symbols correspond to gels previously digested for 1h outside the rheometer. Lines are the best fits of *G'* to a double exponential decay; t_1 and t_2 are the corresponding characteristics decay times.

Fig. 4. Small angle neutron scattering of 10% (w/v) canola gels prepared at pH 8 (closed circles) and at pH 11 (open triangles), before performing digestion experiments. Solid lines represent fits to a double Lorentzian function (see Eq. 1). Inset: Kratky representations of same data (without prefactor, see text at the beginning of section 3.2.).

Fig. 5. SANS of 10% (w/v) canola gels prepared at pH 8: initial sample (black), gastric 30 min (red) and gastric 120 min (yellow). Solid lines represent fits to a double lorentzian function (see Eq. 1). Inset: Kratky representations of same data (without prefactor; see text at the beginning of section 3.2.).

Fig. 6. SANS of 10% (w/v) canola gels prepared at pH 11: initial sample (black), gastric 30 min (red) and gastric 150 min (yellow). Solid lines represent fits to a double Lorentzian function (see Eq. 1). Inset: Kratky representations of same data (without prefactor; see text at the beginning of section 3.2.).

Fig. 7. SANS of 10% (w/v) canola gels prepared at pH 8: initial sample (black), gastric 30 min (red) and gastro 30 min - intestinal 10 min (green). Solid lines represent fits to a double Lorentzian function (see Eq. 1). Inset: Kratky representations of same data (without prefactor; see text at the beginning of section 3.2.).

Fig. 8. SANS of 10% (w/v) canola gels prepared at pH 11: initial sample (black), gastric 30 min (red) and gastro 30 min - intestinal 15 min (blue). Solid lines represent fits to a double Lorentzian function (see Eq. 1). Inset: Kratky representations of same data (without prefactor; see text at the beginning of section 3.2.).

Fig. 9. Diagram presenting the large q scattering parameters: each sample is characterized through a fit to Eq. 1 by the exponent n (in ordinate) and the correlation length ξ. The closed circles represent the gel samples prepared at pH 8 while the open triangles – the ones prepared at pH 11. The numbers indicate the main steps of the digestion sequence (**1** – initial, **2** – gastric 30 min and **3** – gastric 30 min then intestinal 10 min). The colors indicate all the measured digestion steps: orange, red, brown, and yellow correspond to 15, 30, 45 and 120 min of gastric digestion, respectively; dark green, light green, light blue and dark blue – correspond to 30 min gastric step followed by 5, 15 and 30 min of the intestinal step. The crossed symbols represent data from different sets of experiments.

Fig. 10. Schematic representation of a possible formation of the protein gel structures made of cruciferin (shown in orange) and napin (shown in blue), inspired by T. Nicolaï in ref. 58.

Large red squares represent two structure examples: (i) made of the protein beads or (ii) rather spherical protein aggregates resulting from a phase separation (expected in our gels). Small squares are magnifications: proteins at pH 11 - with more compact conformations (violet square, their gel SANS profile is shown by the violet log I vs. log q curve), and proteins at pH 8 - with more unfolded conformations (green square, their gel SANS profile is shown by the green log I vs. log q curve). ξ is the correlation length. The arrow points out the decrease in curves slope at the protein scale when moving from pH 8 (q^{-2}) to pH 11 (q^{-4})."

Table 1. Best fit parameters of SANS curves to the double Lorentzian function (Eq. 1).

Sample name	Correlation length		Exponent		Scale factor	
	Low q Ξ(Å) ±50 Å	High q ξ(Å) ±1 Å	Low q m ±0.1	High q n ±0.1	Low q C ±10%	High q A ±10%
ID 10% pH 8	330	24	4	2.56	340	1.2
ID 10% pH 8 GAS 15 min	370	33	4	2.6	60	1.6
ID 10% pH 8 GAS 30 min	270	33.4	4	2.46	15	1.4
ID 10% pH 8 GAS 45 min	370	36.6	3.85	2.4	30	1.4
ID 10% pH 8 GAS 120 min	270	28	4	2.4	15	1.3
ID 10% pH 8 GAS 30 INT 10 min	250	25.5	4	3.4	80	1
ID 10% pH 8 GAS 30 INT 20 min	260	23	4	3.3	200	1
ID 10% pH 8 GAS 15 INT 30 min	250	28	3.9	3.45	90	2.85
ID 10% pH 11	310	25	4	3.7	900	2
ID 10% pH 11 GAS 15 min	270	32	4	3.1	70	3
ID 10% pH 11 GAS 30 min	250	31	4	3.2	90	4
ID 10% pH 11 GAS 45 min	260	33.5	4	2.9	40	3
ID 10% pH 11 GAS 150 min	320	30.2	4	2.8	60	1
ID 10% pH 11 GAS 30 INT 5 min	270	26	4	3.75	80	2
ID 10% pH 11 GAS 30 INT 10 min	280	26.6	4	3.83	500	1.2
ID 10% pH 11 GAS 30 INT 15 min	270	26	4	3.8	70	1.6
ID 10% pH 11 GAS 30 INT 30 min	260	27	4	3.8	400	1.4
Mel 10% pH 9	770	26	4	2.8	59000	2
Mel 10% pH 11	460	25	3.5	3.9	3000	4
Mel 10% pH 9 GAS 30 min	350	31	4	2.8	2800	1.5
Mel 10% pH 11 GAS 30 min	360	29.5	4	3.9	1000	5

References

[1] Gaudichon, C. (2017). Bioavailability of dietary proteins and amino acids in humans. *XXI Jornadas Nutrición Práctica*, Madrid, Spain. ⟨hal-01569102⟩.

[2] Institute of Medicine (US) Committee on Diet and Health (1992). Chapter 3, The Food We Eat in Woteki, C.E., Thomas, P.R., editors, Eat for Life: The Food and Nutrition Board's Guide to Reducing Your Risk of Chronic Disease, Washington (DC): National Academies Press (US). https://www.ncbi.nlm.nih.gov/books/NBK235023/.

[3] Banerjee, S., & Bhattacharya, S. (2012) Food Gels: Gelling Process and New Applications. *Critical Reviews in Food Science and Nutrition,* 52(4), 334-46. https://doi.org/10.1080/10408398.2010.500234.

[4] Mezzenga, R., & Fischer, P. (2013). The self-assembly, aggregation and phase transitions of food protein systems in one, two and three dimensions. *Reports on Progress in Physics,* 76, 046601. https://doi.org/10.1088/0034-4885/76/4/046601.

[5] Van der Sman, R.G.M., Houlder, S., Cornet, S., & Janssen, A. (2020). Physical chemistry of gastric digestion of proteins gels. *Current Research in Food Science*, 2, 45-60. https://doi.org/10.1016/j.crfs.2019.11.003.

[6] Mehalebi S., Nicolai T., & Durand D. (2008). The influence of electrostatic interaction on the structure and the shear modulus of heat-set globular protein gels. *Soft Matter*, 4, 893. https://doi.org/10.1039/B718640A.

[7] Munialo, C.D., van der Linden, E., Ako, K., & de Jong, H.H.J. (2015). Quantitative analysis of the network structure that underlines the transitioning in mechanical responses of pea protein gel. *Food Hydrocolloids,* 49, 104–117. https://doi.org/10.1016/j.foodhyd.2015.03.018.

[8] Sarwar Gilani, G., Wu Xiao, C., & Cockell, K.A. (2012). Impact of antinutritional factors in food proteins on the digestibility of protein and the bioavailability of amino acids and on protein quality. *British Journal of Nutrition,* 108, 315-332. https://doi.org/10.1017/S0007114512002371.

[9] Guillamón, E., Pedrosa, M. M., Burbano, C., Cuadrado, C., de Cortes Sánchez, M., & Muzquiz, M. (2008). The trypsin inhibitors present in seed of different grain legume species and cultivar. *Food Chemistry*, 107(1), 68–74. https://doi.org/10.1016/j.foodchem.2007.07.029.

[10] Hertzler S.R., Lieblein-Boff J.C., Weiler M., & Allgeier C. (2020). Plant Proteins: Assessing Their Nutritional Quality and Effects on Health and Physical Function. *Nutrients*, 12(12), 3704. https://doi.org/10.3390/nu12123704.

[11] Tomé, D. (2013). Digestibility issues of vegetable versus animal proteins: Protein and amino acid requirements-functional aspects. *Food and Nutrition Bulletin*, 34, 272-274. https://doi.org/10.1177/156482651303400225.

[12] Luo, N., Ye, A., Wolber, F.M., & Singh, H. (2021). Effect of Gel Structure on the In Vitro Gastrointestinal Digestion Behaviour of Whey Protein Emulsion Gels and the Bioaccessibility of Capsaicinoids. *Molecules*, 26, 1379. https://doi.org/10.3390/molecules26051379.

[13] Fardet, A., Dupont, D., Rioux, L., & Turgeon, S.L. (2019). Influence of food structure on dairy protein, lipid and calcium bioavailability: A narrative review of evidence. *Critical Reviews in Food Science and Nutrition*, 59(13). https://doi.org/10.1080/10408398.2018.1435503.

[14] Singh, H., Ye, A., & Ferrua, M.J. (2015). Aspects of food structures in the digestive tract. *Current Opinion in Food Science*, 3, 85-93. https://doi.org/10.1016/j.cofs.2015.06.007.

[15] Boirie, Y., Dangin, M., Gachon, P, Vasson, M.P., Maubois J.L., & Beaufrère, B. (1997). Slow and fast dietary proteins differently modulate postprandial protein accretion. *Proceedings of the National Academy of Sciences of the United States of America*, 94(26), 14930-5. https://doi.org/10.1073/pnas.94.26.14930.

[16] Dupont, D. (2020). Time profile of blood amino acids content after digestion of milk /dairy gels, in Dupont, D., & Tomé D., Editors, Milk proteins: Digestion and absorption in the gastrointestinal tract. *Academic Press*. Third Edition, Elsevier, Milk Proteins From Expression to Food, 978-0128152515. https://doi.org/10.1016/B978-0-12-815251-5.00020-7.

[17] Guo, Q., Ye, A., Lad, M., Dalgleish, D. & Singh, H. (2014). Effect of gel structure on the gastric digestion of whey protein emulsion gels. *Soft Matter*, 10, 1214-1223. https://doi.org/10.1039/C3SM52758A.

[18] Somaratne, G., Nau, F., Ferrua, M.J., Singh, J., Ye, A., Dupont, D., Singh, R.P, & Floury, J. (2020). In-situ disintegration of egg white gels by pepsin and kinetics of nutrient release followed by time-lapse confocal microscopy. *Food Hydrocolloids*, 98, 105228. https://doi.org/10.1016/j.foodhyd.2019.105228.

[19] Thévenot, J., Cauty, C., Legland, D., Dupont, D., & Floury, J. (2017). Pepsin diffusion in dairy gels depends on casein concentration and microstructure. *Food Chemistry*, 223, 54-61. https://doi.org/10.1016/j.foodchem.2016.12.014.

[20] Luo, Q, Boom, R.M., & Janssen, A.E.M. (2015). Digestion of protein and protein gels in simulated gastric environment. *LWT Food Science and Technology*, *63*(1), 161-168. https://doi.org/10.1016/j.lwt.2015.03.087.

[21] Opazo-Navarrete, M., Altenburg, M.D., Boom, R.M, & Janssen AEM. (2018). The Effect of Gel Microstructure on Simulated Gastric Digestion of Protein Gels. *Food Biophysics,* 13, 124–138. https://doi.org/10.1007/s11483-018-9518-7.

[22] Johnston, N., Dettmar, P.W., Bishwokarma, B., Lively, M.O., & Koufman J.A. (2007). Activity/stability of human pepsin: implications for reflux attributed laryngeal disease. *Laryngoscope*, 117(6), 1036-9. https://doi.org/10.1097/MLG.0b013e31804154c3.

[23] Piper, D.W., & Fenton, B.H. (1965). pH stability and activity curves of pepsin with special reference to their clinical importance, *Gut*, 6 (5), 506-508. https://doi.org/10.1136/gut.6.5.506.

[24] Cox, M., Nelson, D.R. (2008). Principles of biochemistry (4th ed.). Lehninger (Chapter 2). Enzymes. (pp. 212).

[25] Bornhorst, G.M., Rutherfurd, S.M., Roman, M.J., Burri, B.J., Moughan, P.J., & Singh, R.P. (2014). Gastric pH Distribution and Mixing of Soft and Rigid Food Particles in the Stomach using a Dual-Marker Technique. *Food Biophysics*, 9 (3), 292-300. https://doi.org/10.1007/s11483-014-9354-3.

[26] Floury, J., Bianchi, T., Thévenot, J., Dupont, D., Jamme, F., Lutton, E. & Le Feunteun, S. (2018). Exploring the breakdown of dairy protein gels during in vitro gastric digestion using time-lapse synchrotron deep-UV fluorescence microscopy, *Food Chemistry*, 239, 898-910, https://doi.org/10.1016/j.foodchem.2017.07.023.

[27] Fruton, J.S. (1970). The specificity and mechanism of pepsin action. *Advances in Enzymology and Related Areas of Molecular Biology*, 33, 401–443.

[28] Berg, J.M., Tymoczko, J.L., Stryer, L. (2002). Biochemistry. (5th ed.). (Section 23.1). Proteins Are Degraded to Amino Acids. Available from: https://www.ncbi.nlm.nih.gov/books/NBK22600/.

[29] Betz, M., Hörmansperger, J., Fuchs, T., Kulozik, U. (2012). Swelling behaviour, charge and mesh size of thermal protein hydrogels as influenced by pH during gelation. *Soft Matter*, 8, 2477-2485. https://doi.org/10.1039/C2SM06976H.

[30] Wanasundara, J.P.D., McIntosh, T.C., Perera, S.P., Thushan, S. Withana-Gamage, T.S. & Mitra, P. (2016). Canola/rapeseed protein-functionality and nutrition. *OCL-Oilseeds and fats, Crops and Lipids*, 23 (4) D407. https://doi.org/10.1051/ocl/2016028.

[31] Fleddermann, M., Fechner, A., Rößler, A., Bähr, M., Pastor, A., Liebert, F. & Jahreis, G. (2012). Nutritional evaluation of rapeseed protein compared to soy protein for quality, plasma amino acids, and nitrogen balance - a randomized cross-over intervention study in humans. *Clinical Nutrition,* 32(4), 519-26. https://doi.org/10.1016/j.clnu.2012.11.005.

[32] *Protein and amino acid requirements in human nutrition.* Report of a joint FAO/WHO/UNU Expert Consultation. Geneva: WHO; 2007. Report no. 724. In press 2007. Available from: http://apps.who.int/iris/bitstream/10665/43411/1/WHO_TRS_935_eng.pdf?ua=1.

[33] Bos, C., Airinei, G., Mariotti, F., Benamouzig, R., Bérot, S., Evrard, J., Fénart, E., Tomé, D. & Gaudichon, C. (2007). The Poor Digestibility of Rapeseed Protein Is Balanced by Its Very High Metabolic Utilization in Humans. *The Journal of Nutrition*, 137, 594-600. https://doi.org/10.1093/jn/137.3.594.

[34] Bayrak, M., Mata, J., Raynes, J.K., Greaves, M., White, J., Conn, C.J., Floury, J., Logan, A. (2021). Investigating casein gel structure during gastric digestion using ultra-small and small-angle neutron scattering. *Journal of Colloid and Interface Science*, 594, 561-574. https://doi.org/10.1016/j.jcis.2021.03.087.

[35] Devle, H., Rukke, E.O., Vegarud, G., Naess-Andresen, C. F., Schüller, R., & Ekeberg, D. (2012). Rheological characterization of milk during digestion with human gastric and duodenal enzymes. *Annual Transactions of the Nordic Rheology Society*, 20, 271-276.

[36] Pink, D.L., Foglia, F., Barlow, D.J., Lawrence, M.J., & Lorenz, C.D. (2021). The Impact of Lipid Digestion on the Dynamic and Structural Properties of Micelles. *Small*, 17(6), 2004761. https://doi.org/10.1002/smll.202004761.

[37] Rezhdo, O., Di Maio, S., Le, P., Littrell, K.C., Carrier, R.L., & Chen, S.H. (2017). Characterization of colloidal structures during intestinal lipolysis using small-angle neutron scattering. *Journal of colloid and interface science*, 499, 189–201. https://doi.org/10.1016/j.jcis.2017.03.109.

[38] Espert, M., Salvador, A., Sanz, T. (2016). In vitro digestibility of highly concentrated methylcellulose O/W emulsions: rheological and structural changes. *Food Function*, 7(9), 3933-3942. https://doi.org/10.1039/C6FO00888G.

[39] Pasquier, J., Brûlet, A., Boire, A., Jamme, F., Perez, J., Bizien, T., Lutton, E. & Boué, F. (2019). Monitoring food structure during digestion using small-angle scattering and imaging techniques. *Colloids and Surfaces A: Physicochemical and Engineering Aspects*, 570, 96-106. https://doi.org/10.1016/j.colsurfa.2019.02.059.

[40] Ainis, W., Ersch, C., & Ipsen, R. (2018). Partial replacement of whey proteins by rapeseed proteins in heat-induced gelled systems: Effect of pH. *Food Hydrocolloids*, 77, 397-406. https://doi.org/10.1016/j.foodhyd.2017.10.016.

[41] Schwenke, K.D., Raab, B., Plietz, P., & Damaschun G. (1983). The structure of the 12S globulin from rapeseed. *Nahrung.* 27, 165–175. https://doi.org/10.1002/food.19830270208.

[42] Schwenke, K.D., Raab, B., Linow, K.J., Pahtz, W., & Uhlig, J. (1981). Isolation of the 12S globulin from rapeseed (Brassica napus L.) and characterization as a "neutral" protein. On seed proteins. Part 13. *Nahrung,* 25, 271–280.

[43] Lönnerdal, B., & Janson, J.C. (1972). Studies on Brassica seed proteins: I. The low molecular weight proteins in rapeseed. Isolation and characterization. *BBA-Protein Structure*, 278, 175–183.

[44] Pedroche, J., Yust, M.M., Lqari, H., Girón-Calle, J., Alaiz, M., Vioque, J., & Millán, F. (2004). Brassica carinata protein isolates: Chemical composition, protein characterization and improvement of functional properties by protein hydrolysis. *Food Chemistry*, 88, 337–346. https://doi.org/10.1016/j.foodchem.2004.01.045.

[45] Shewry, P.R., Napier, J.A., & Tatham, A.S. (1995). Seed storage proteins: Structures and biosynthesis. *The Plant Cell*, 7, 945–956. https://doi.org/10.1105/tpc.7.7.945.

[46] Bérot, S., Compoint, J.P., Larré, C., Malabat, C., Guéguen J. (2005). Large scale purification of rapeseed proteins (Brassica napus L.). *Journal of Chromatography B*, 818, 35-42, https://doi.org/10.1016/j.jchromb.2004.08.001.

[47] Minekus, M., Alminger, M., Alvito, P., Ballance, S., Bohn, T., Bourlieu, C., Carrière, F., Boutrou, R., Corredig, M., Dupont, D., Dufour, C., Egger, L., Golding, M., Karakaya, S.,

Kirkhus, B., Le Feunteun, S., Lesmes, U., Macierzanka, A., Mackie, A., Marze, S., McClements, D.J., Ménard, O., Recio, I., Santos, C.N., Singh, R.P., Vegarud G.E., Wickham M.S., Weitschies W. & Brodkorb, A. (2014). A standardised static in vitro digestion method suitable for food - an international consensus. *Food Function*, 5, 1113-1124. https://doi.org/10.1039/c3fo60702j.

[48] Brodkorb, A., Egger, L., Alminger, M. *et al.* (2019). INFOGEST static in vitro simulation of gastrointestinal food digestion. *Nature Protocols,* 14, 991–1014. https://doi.org/10.1038/s41596-018-0119-1.

[49] Boyer, J.L. (2013). Bile formation and secretion. *Comprehensive Physiology*, 3, 1035-1078. https://doi.org/10.1002/cphy.c120027.

[50] Maldonado-Valderrama, J., Wilde, P., Macierzanka, A., Mackie, A. (2011). The role of bile salts in digestion. *Advances in Colloid and Interface Science*, 165, 36-46. https://doi.org/10.1016/j.cis.2010.12.002.

[51] Gass, J., Vora, H., Hofmann, A.F., Gray, G.M., Khosla, C. (2007). Enhancement of dietary protein digestion by conjugated bile acids. *Gastroenterology,* 133, 16-23. https://doi.org/10.1053/j.gastro.2007.04.008.

[52] Brûlet, A., Lairez, D., Lapp, A., Cotton, J.-P. (2007). Improvement of data treatment in SANS. *Journal of Applied Crystallography,* 40, 165-177. https://doi.org/10.1107/S0021889806051442

[53] http://www.sasview.org.

[54] Mezger, T.G. (2006). The rheology handbook: for users of rotational and oscillatory rheometers. (2nd ed.). Hannover: Vincentz Network GmbH and Co KG.

[55] Huang, T., Tu, Z.C., Wang, H., Liu, W., Zhang, L., Zhang, Y. & ShangGuan, X. (2017). Comparison of rheological behaviors and nanostructure of bighead carp scales gelatin modified by different modification methods. *Journal of Food Science and Technology*, 5, 1256-1265. https://doi.org/10.1007/s13197-017-2511-1.

[56] Léger, L.W. & Arntfield, S.D. (1993). Thermal gelation of the 12S canola globulin. *Journal of the American Oil Chemists' Society,* 70, 853–861. https://doi.org/10.1007/BF02545343.

[57] Yang, C., Wang, Y., Vasanthan, T., Chen, L. (2014). Impacts of pH and heating temperature on formation mechanisms and properties of thermally induced canola protein gels. *Food Hydrocolloids*, 40(10), 225-236. https://doi.org/10.1016/j.foodhyd.2014.03.011.

[58] Nicolai, T. (2019). Gelation of food protein-protein mixtures. *Advances in Colloid and Interface Science*, 270, 147-164. https://doi.org/10.1016/j.cis.2019.06.006.

[59] Tarhan, O., Spotti, M.J., Schaffter, S., Corvalan, C.M. & Campanella, O.H. (2016). Rheological and structural characterization of whey protein gelation induced by enzymatic hydrolysis. *Food Hydrocolloids*, 61, 211-220. https://doi.org/10.1016/j.foodhyd.2016.04.042.

[60] De Maria, S., Ferrari, G. & Maresca, P. (2015). Rheological Characterization Bovine Serum Albumin Gels Induced by High Hydrostatic Pressure. *Food and Nutrition Sciences*, 6, 770-779. https://doi.org/10.4236/fns.2015.69080.

[61] Siong, H.T., Mailer, R.J., Blanchard, C.L., Agboola, S.O., Day, L. (2014). Gelling properties of protein fractions and protein isolate extracted from Australian canola meal. *Food Research International*, 62, 819-828. https://doi.org/10.1016/j.foodres.2014.04.055.

[62] Zhou, H.X., & Pang, X. (2018). Electrostatic Interactions in Protein Structure, Folding, Binding, and Condensation. *Chemical Reviews*, 118, 1691-1741. https://doi.org/10.1021/acs.chemrev.7b00305.

[63] Yan, Y.B, Wang, Q., He, H.W., Zhou, H.M. (2004). Protein thermal aggregation involves distinct regions: sequential events in the heat-induced unfolding and aggregation of hemoglobin. *Biophysical Journal*, 86(3), 1682-1690. https://doi.org/10.1016/S0006-3495(04)74237-X.

[64] Montellano Duran, N., Galante, M., Spelzini, D., Boeris, V. (2018). The effect of carrageenan on the acid-induced aggregation and gelation conditions of quinoa proteins. *Food Research International*, 107, 683-690. http://dx.doi.org/10.1016/j.foodres.2018.03.015.

[65] Van Camp, J., Huyghebaert, A. (1995). A comparative rheological study of heat and high pressure induced whey protein gels. *Food Chemistry*, 54, 357-364. https://doi.org/10.1016/0308-8146(95)00040-P.
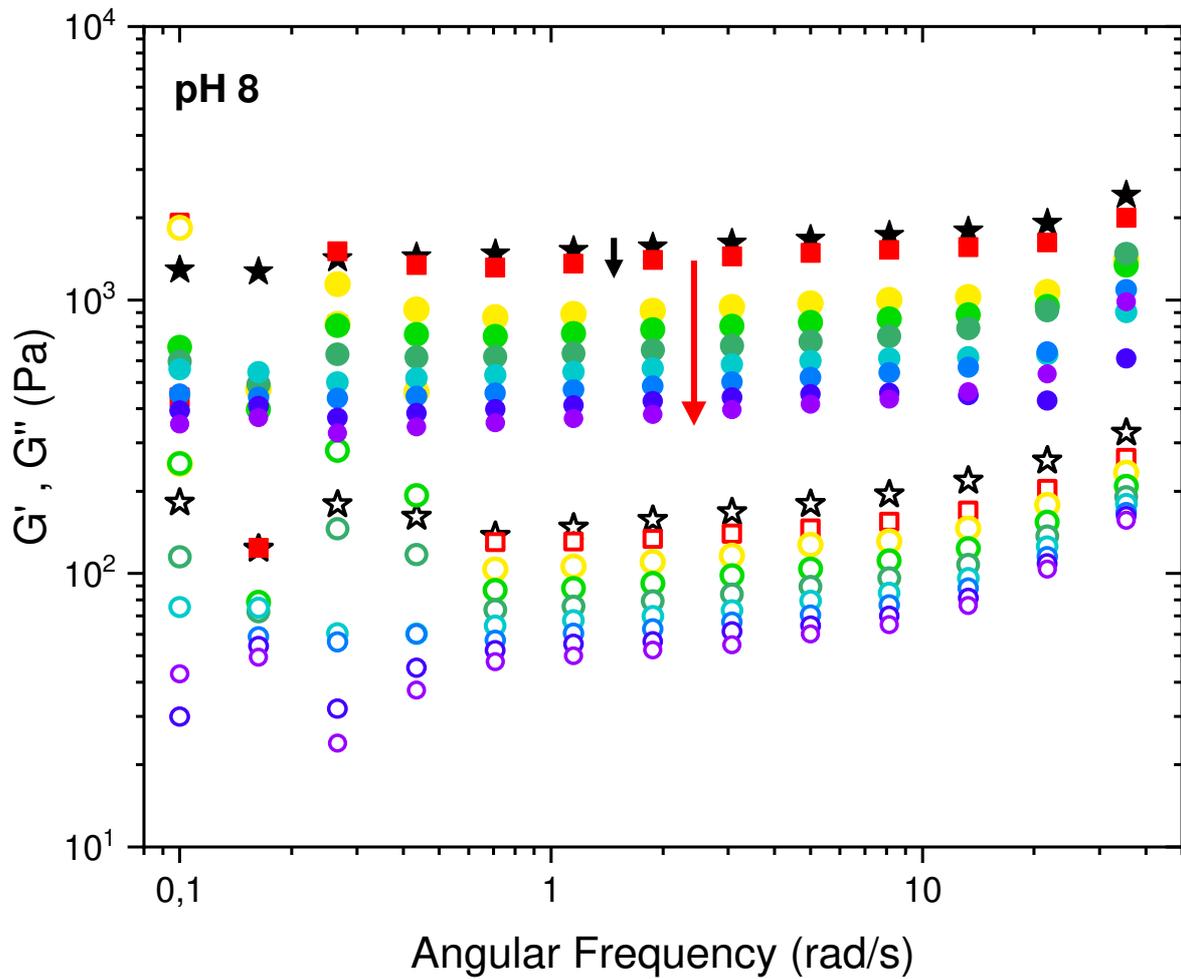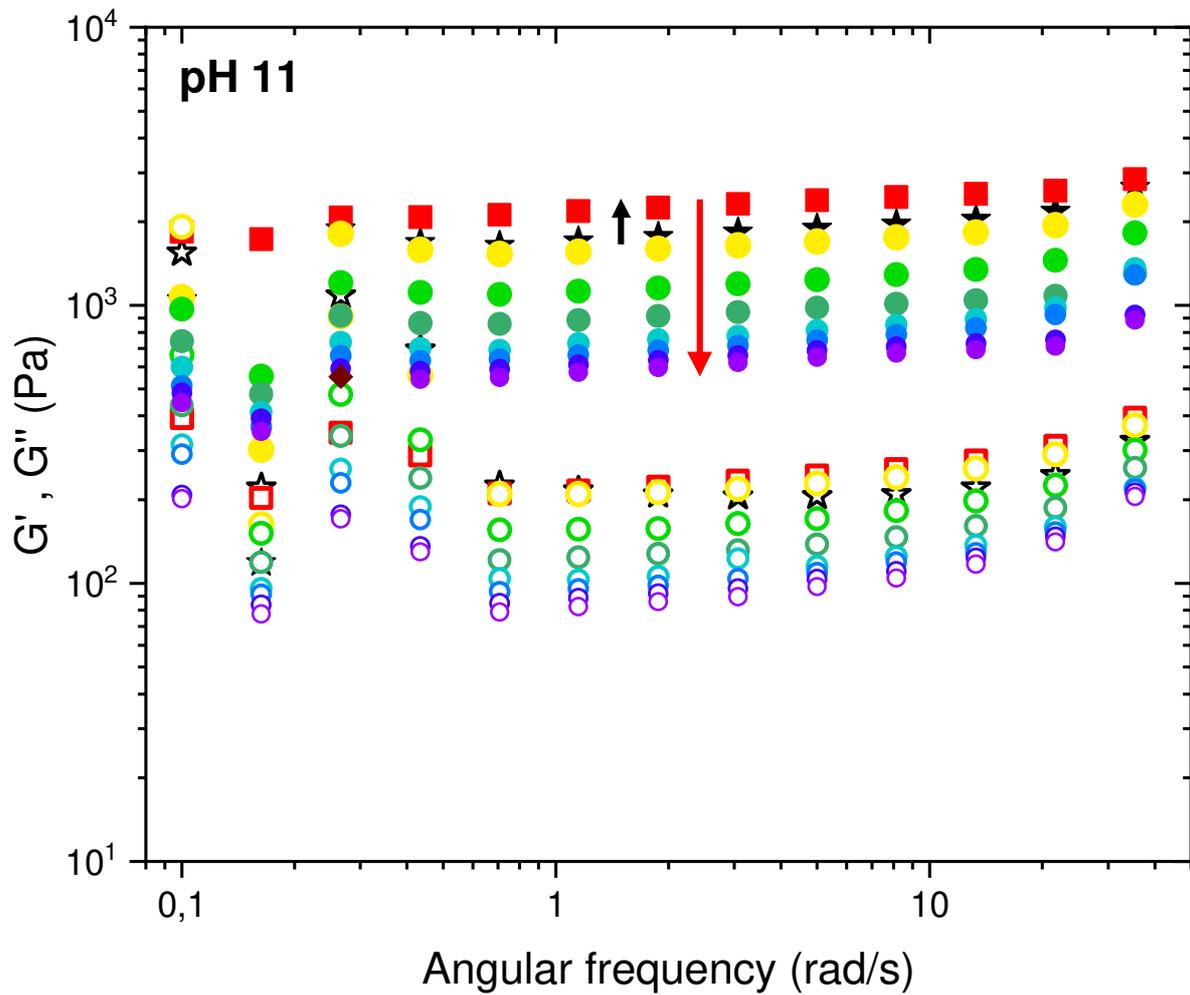
Figure 1. Frequency sweep tests on the canola protein gel prepared at pH 8 (100 g/L) during the digestion process at 37°C: storage moduli (*G'*, closed symbols) and loss moduli (*G''*, open symbols) as a function of oscillating frequency (0.1-50 rad/s). The arrows indicate the direction

of the digestion: 1st step – from initial gel (black stars) to 30' of gastric digestion (red squares),

2nd step – intestinal digestion kinetics during 60' (t_0 – yellow circles, t_{60} – violet circles); duration of one sweep was ~10 min.

Figure 2. Frequency sweep tests on the canola protein gel prepared at pH 11 (100 g/L) during the digestion process at 37°C: storage moduli (G', closed symbols) and loss moduli (G'', open symbols) as a function of oscillating frequency (0.1-50 rad/s). The arrows indicate the direction of the digestion: 1st step – from initial gel (black stars) to 30 min of gastric digestion (red squares), 2nd step – intestinal digestion kinetics during 60 min (t_0 – yellow circles, t_{60} – violet circles); duration of one sweep was ~10 min.
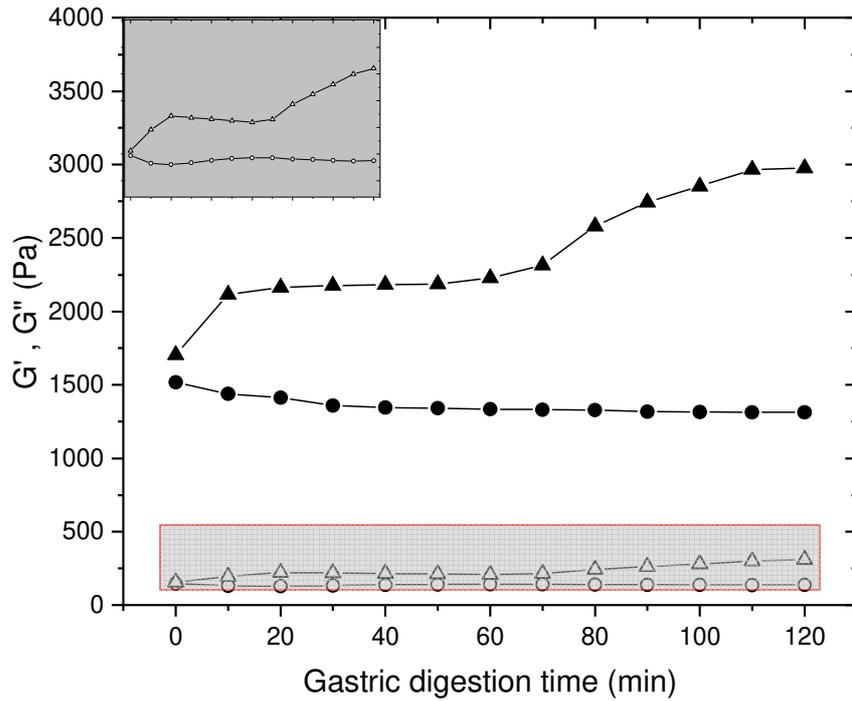
Figure 3 a. Variations of *G'* (closed symbols) and *G''* (open symbols) at a frequency of 1.15 rad/s as function of gastric digestion time. Round symbols - pH 8; triangles - pH 11. Inset: close-up on variations of *G''*.
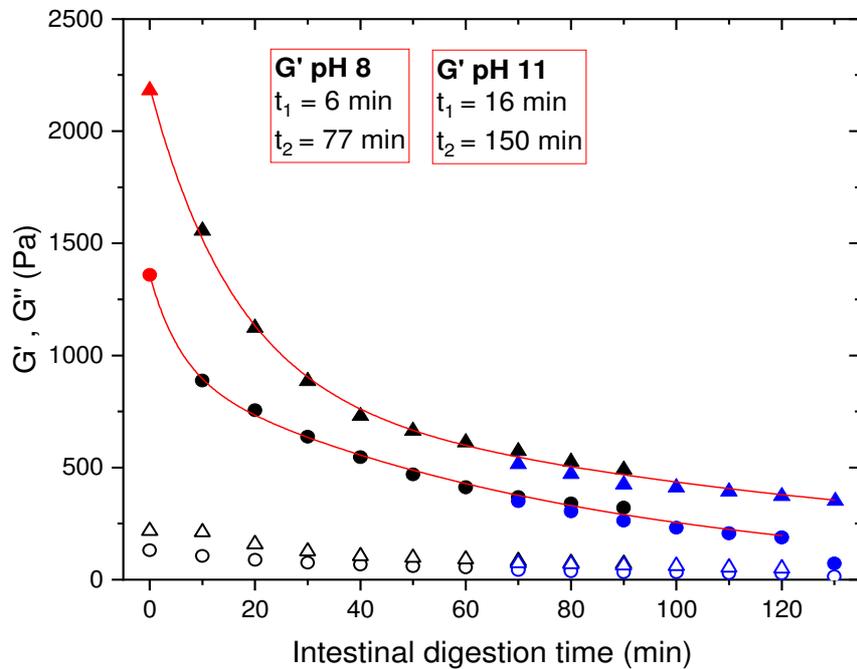

Figure 3 b. Variations of *G'* (closed symbols) and *G''* (open symbols) at frequency of 1.15 rad/s as function of intestinal digestion time. Round symbols - pH 8; triangles - pH 11. Blue symbols correspond to gels previously digested for 1h outside the rheometer. Lines are the best fits of *G'* to a double exponential decay; t_1 and t_2 are the corresponding characteristics decay times.
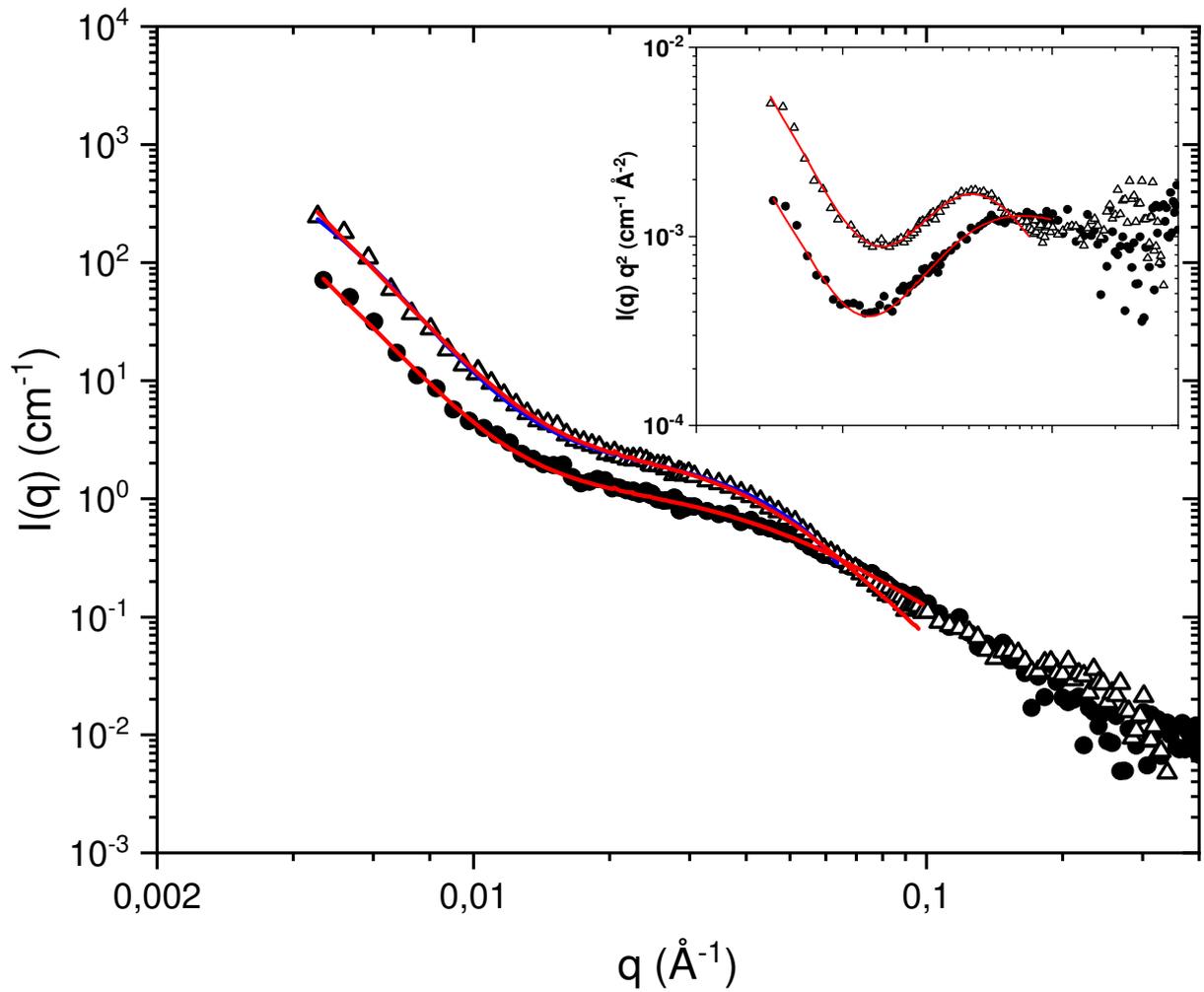
Figure 4. Small angle neutron scattering of 10% (w/v) canola gels prepared at pH 8 (closed circles) and at pH 11 (open triangles), before performing digestion experiments. Solid lines represent fits to a double Lorentzian function (see Eq. 1). Inset: Kratky representations of same data (without prefactor, see text at the beginning of section 3.2.).
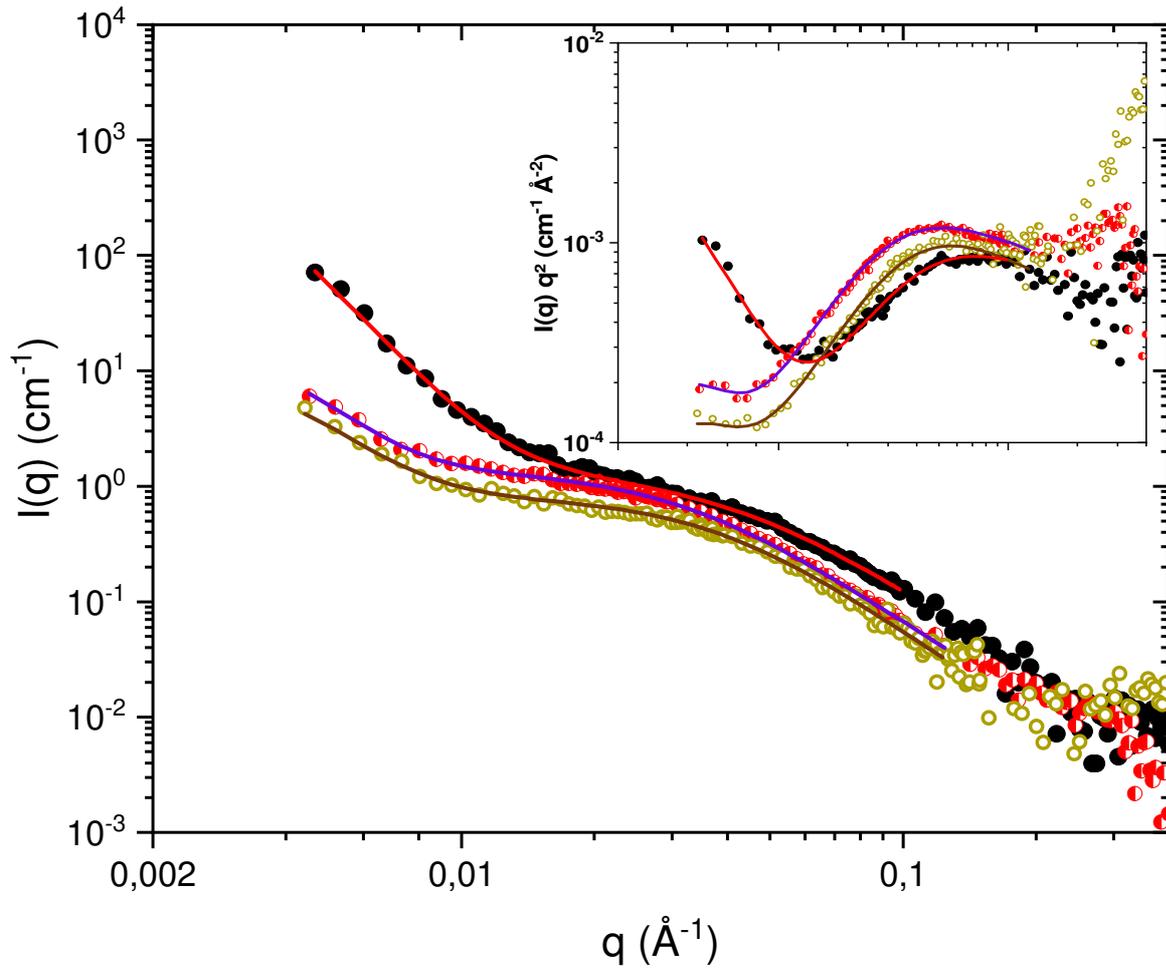
Figure 5. SANS of canola protein gels prepared at pH 8 (100 g/L): initial sample (black), gastric 30 min (red) and gastric 120 min (dark yellow). Solid lines represent fits to a double Lorentzian function (see Eq. 1). Inset: Kratky representations of same data (without the prefactor; see text at the beginning of section 3.2.).
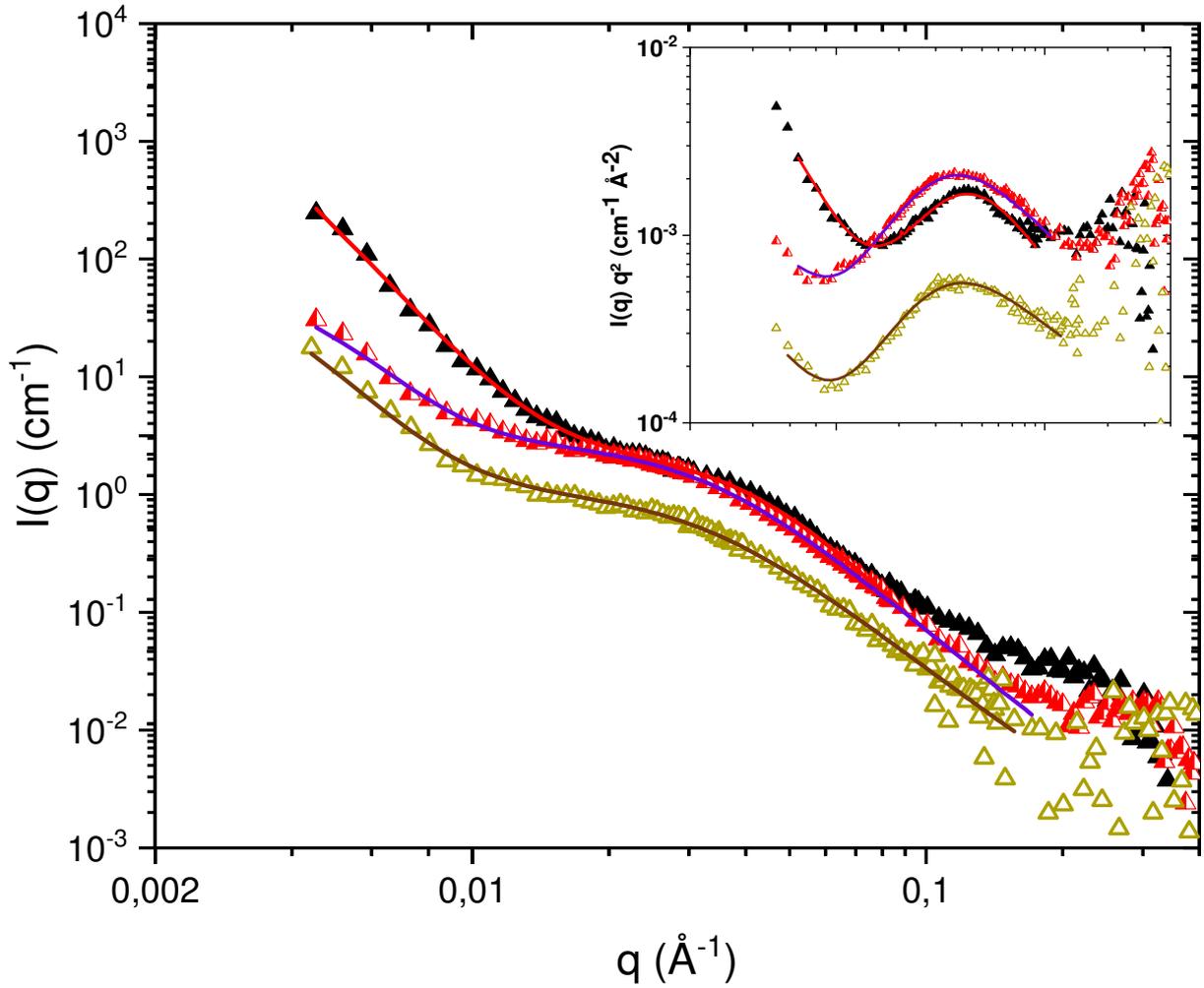
Figure 6. SANS of canola protein gels prepared at pH 11 (100 g/L): initial sample (black), gastric 30 min (red) and gastric 150 min (dark yellow). Solid lines represent fits to a double Lorentzian function (see Eq. 1). Inset: Kratky representations of same data (without the prefactor; see text at the beginning of section 3.2.).
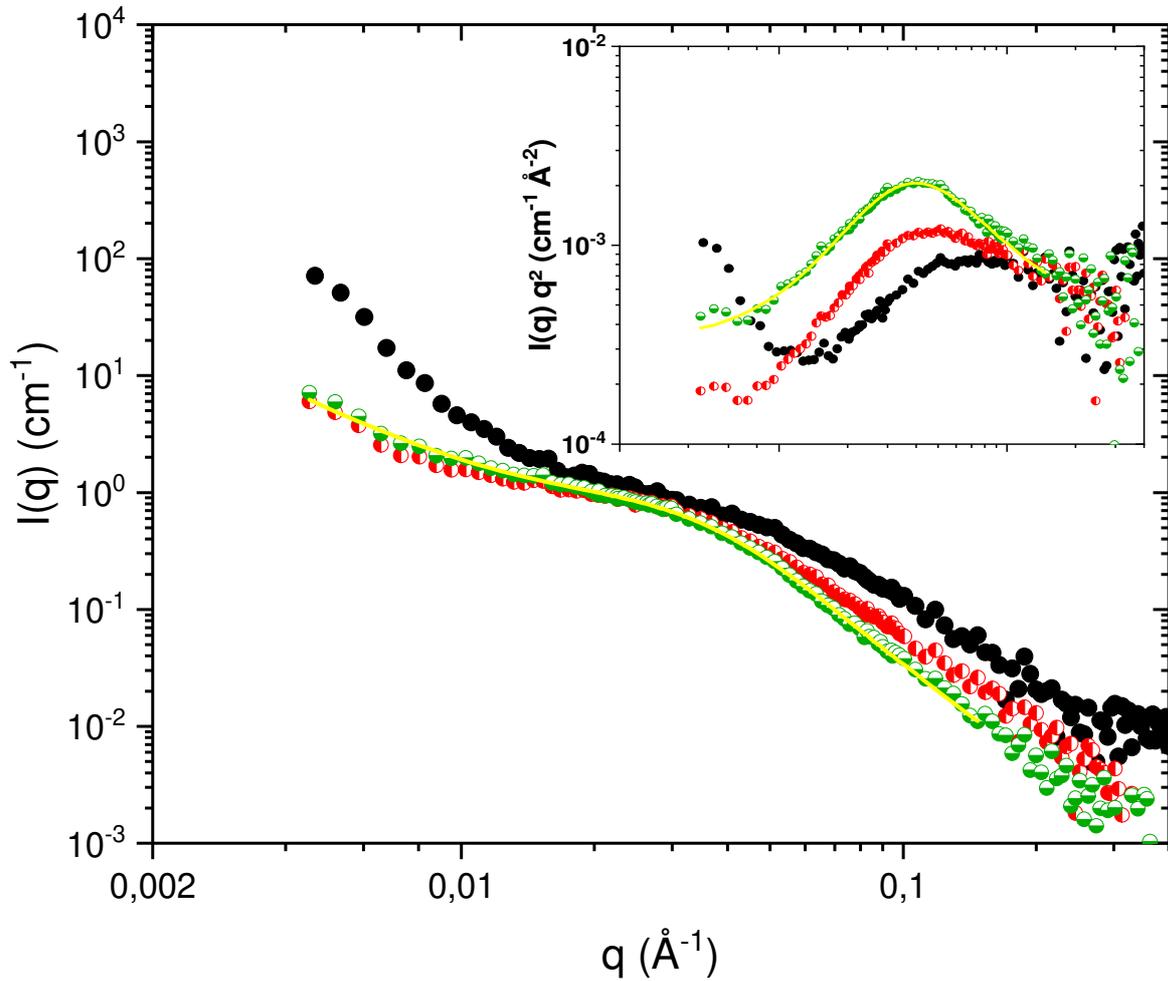
Figure 7. SANS of canola protein gels prepared at pH 8 (100 g/L): initial sample (black), gastric 30 min (red) and gastro 30 min - intestinal 10 min (green). Solid lines represent fits to a double Lorentzian function (see Eq. 1). Inset: Kratky representations of same data (without the prefactor; see text at the beginning of section 3.2.).

Figure 8. SANS of canola protein gels prepared at pH 11 (100 g/L): initial sample (black), gastric 30 min (red) and gastro 30 min - intestinal 15 min (blue). Solid lines represent fits to a double Lorentzian function (see Eq. 1). Inset: Kratky representations of same data (without the prefactor; see text at the beginning of section 3.2.).
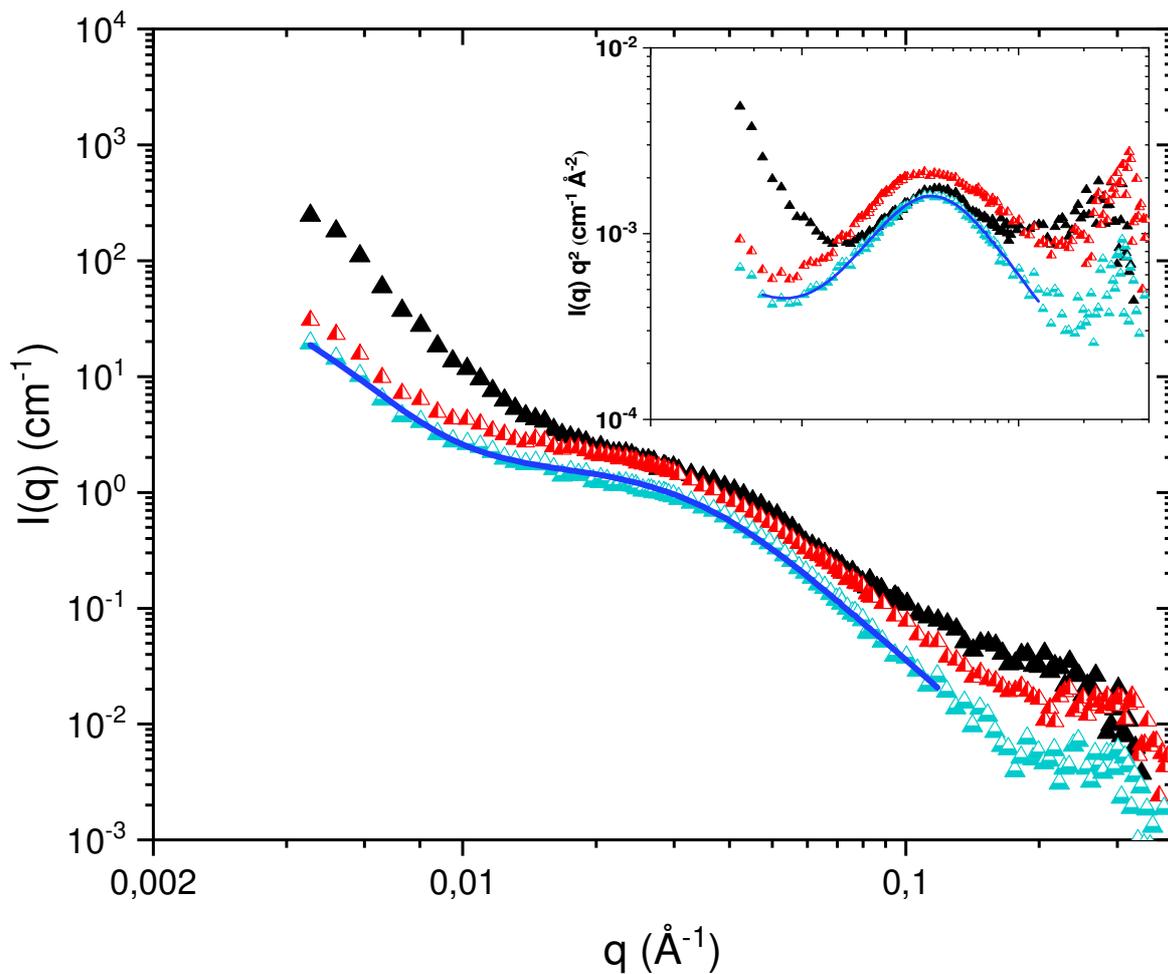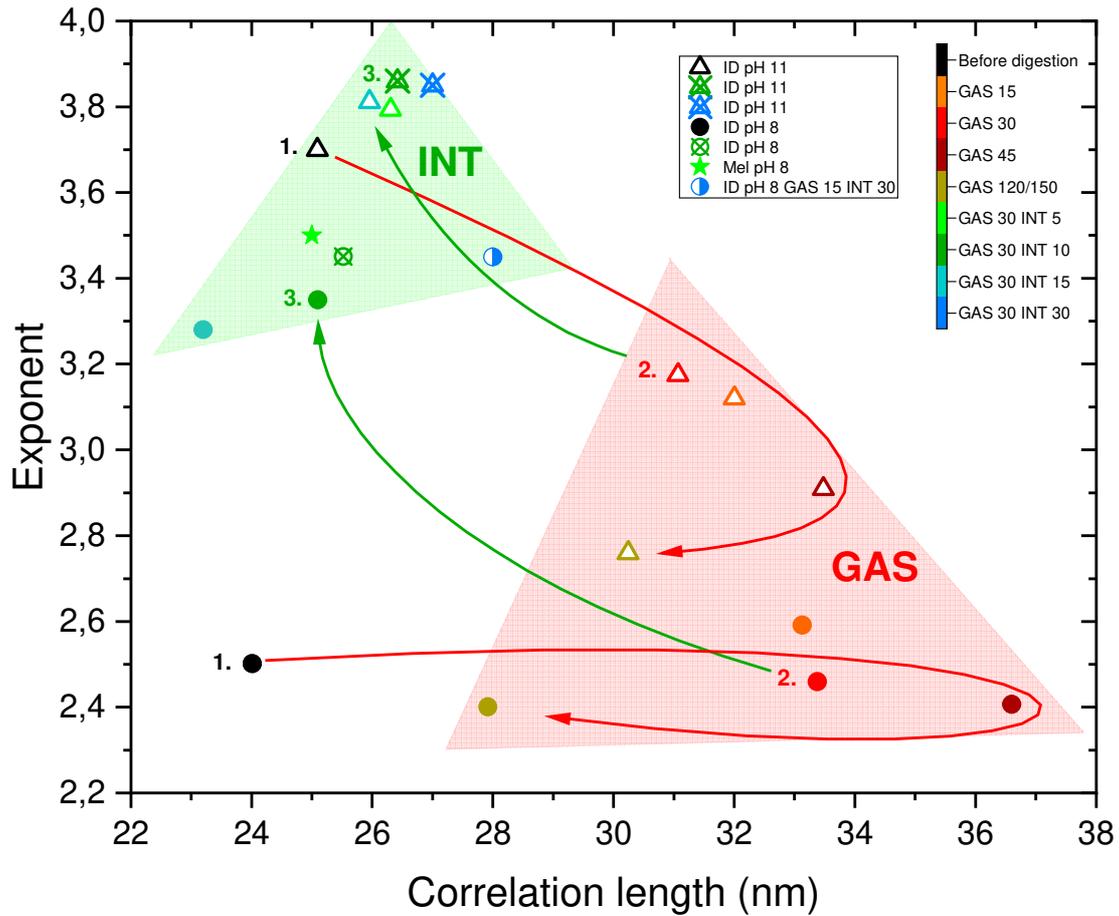
Figure 9. Diagram presenting the large *q* scattering parameters: each sample is characterized through a fit to Eq. 1 by the exponent *n* (in ordinate) and the correlation length ξ. The closed circles represent the gel samples prepared at pH 8 while the open triangles – the ones prepared at pH 11. The numbers indicate the main steps of the digestion sequence (**1** – initial, **2** – gastric 30 min and **3** – gastric 30 min then intestinal 10 min). The colors indicate all the measured digestion steps: orange, red, brown and yellow correspond to 15, 30, 45

and 120 min of gastric digestion, respectively; dark green, light green, light blue and dark blue – correspond to 30 min gastric step followed by 5, 15 and 30 min of the intestinal step. The crossed symbols represent data from different sets of experiments.
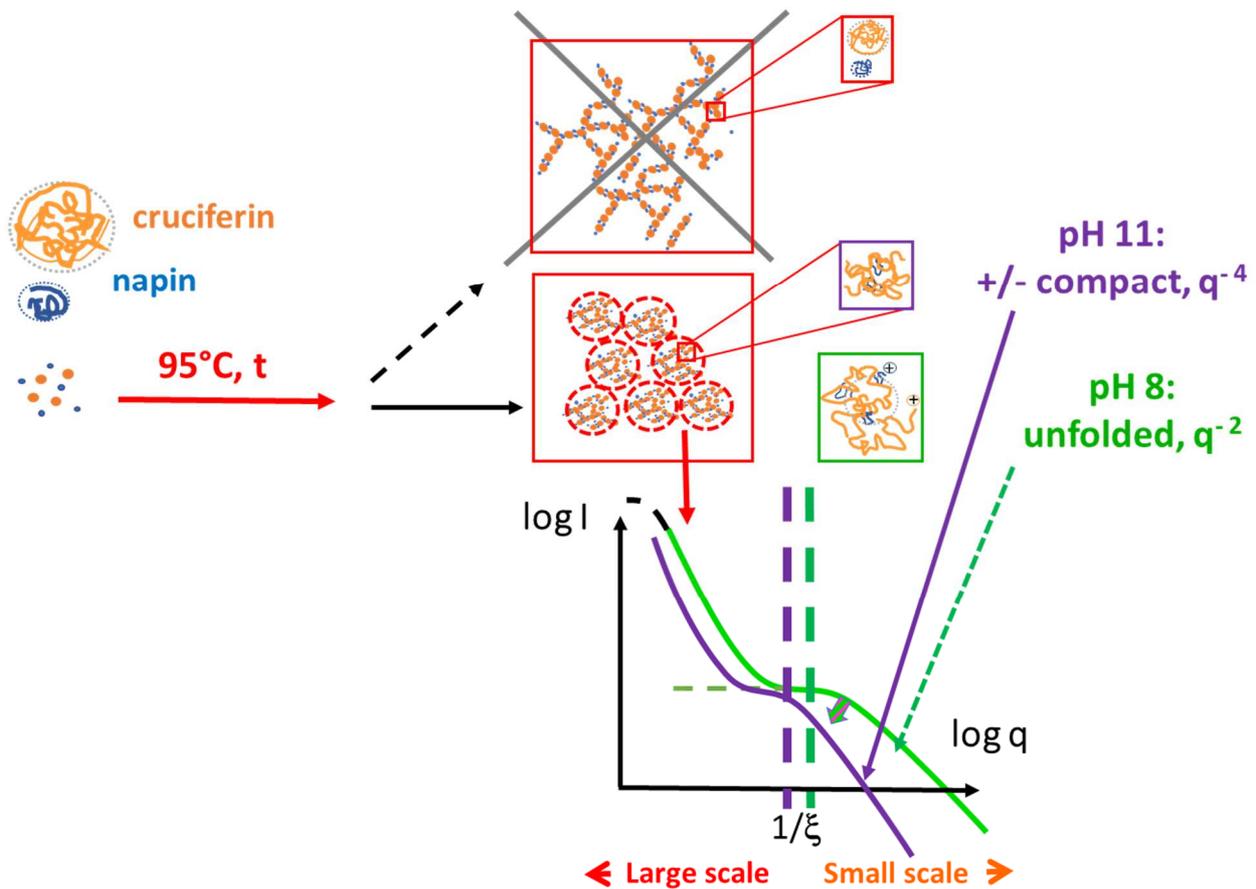
Figure 10. Schematic representation of a possible formation of the protein gel structures made of cruciferin (shown in orange) and napin (shown in blue), inspired by T. Nicolaï in ref. 58. Large red squares represent two structure examples: (i) made of the protein beads or (ii) rather spherical protein aggregates resulting from a phase separation (expected in our gels). Small squares are magnifications: proteins at pH 11 - with more compact conformations (violet square, their gel SANS profile is shown by the violet log I vs. log q curve), and proteins at pH 8 - with more unfolded conformations (green square, their gel SANS profile is shown by the green log I vs. log q curve). ξ is the correlation length. The arrow points out the decrease in curves slope at the protein scale when moving from pH 8 (q^{-2}) to pH 11 (q^{-4}).

Table 1. Best fit parameters of SANS curves to the double lorentzian function (Eq. 1).

Sample name	Correlation length		Exponent		Scale factor	
	Low q Ξ(Å) ±50 Å	**High q** ξ(Å) ±1 Å	**Low q** *m* ±0.1	**High q** *n* ±0.1	**Low q** *C* ±10%	**High q** *A* ±10%
ID 10% pH 8	330	24	4	2.56	340	1.2
ID 10% pH 8 GAS 15 min	370	33	4	2.6	60	1.6
ID 10% pH 8 GAS 30 min	270	33.4	4	2.46	15	1.4
ID 10% pH 8 GAS 45 min	370	36.6	3.85	2.4	30	1.4
ID 10% pH 8 GAS 120 min	270	28	4	2.4	15	1.3
ID 10% pH 8 GAS 30 INT 10 min	250	25.5	4	3.4	80	1
ID 10% pH 8 GAS 30 INT 20 min	260	23	4	3.3	200	1
ID 10% pH 8 GAS 15 INT 30 min	250	28	3.9	3.45	90	2.85
ID 10% pH 11	310	25	4	3.7	900	2
ID 10% pH 11 GAS 15 min	270	32	4	3.1	70	3
ID 10% pH 11 GAS 30 min	250	31	4	3.2	90	4
ID 10% pH 11 GAS 45 min	260	33.5	4	2.9	40	3
ID 10% pH 11 GAS 150 min	320	30.2	4	2.8	60	1
ID 10% pH 11 GAS 30 INT 5 min	270	26	4	3.75	80	2
ID 10% pH 11 GAS 30 INT 10 min	280	26.6	4	3.83	500	1.2
ID 10% pH 11 GAS 30 INT 15 min	270	26	4	3.8	70	1.6
ID 10% pH 11 GAS 30 INT 30 min	260	27	4	3.8	400	1.4
Mel 10% pH 9	770	26	4	2.8	59000	2
Mel 10% pH 11	460	25	3.5	3.9	3000	4
Mel 10% pH 9 GAS 30 min	350	31	4	2.8	2800	1.5
Mel 10% pH 11 GAS 30 min	360	29.5	4	3.9	1000	5